

ZAMM · Z. Angew. Math. Mech. **81** (2001) 2, 99–118

FRIGAARD, I. A.; SCHERZER, O.; SONA, G.

Uniqueness and Non-uniqueness in the Steady Displacement of Two Visco-plastic Fluids

We study steady miscible displacements of two visco-plastic fluids in a long plane channel. If the yield stress of the displacing fluid is less than that of the displaced fluid, uniform static residual layers can be left attached to the walls of the channel as the displacement front propagates steadily. We investigate this steady finger propagation and the problem of finger width selection. The problem is fully two-dimensional, with the two fluids separated by a sharp interface. For a given fixed interface, chosen from a wide class of physically sensible interface shapes, we show that there exists a unique solution. As well as flexibility in the exact shape of the interface, the residual static layer thickness is also non-unique. Typically layer thicknesses $h \in (h_{\min}, h_{\max})$ admit a physically sensible static layer solution, where h_{\min} and h_{\max} are easily computable functions of the dimensionless problem parameters. The dependency of h_{\min} and h_{\max} on the dimensionless problem parameters is explained and example solutions are computed for different static residual thicknesses.

Key words: finger-width selection, visco-plastic fluid, variational inequality, existence and uniqueness

MSC (2000): 35A15, 35R35, 76A05, 76M30, 76T99

1. Introduction

This paper considers the mathematical theory underlying a particular type of *viscous-fingering*, namely the formation of static residual layers on the walls of a plane channel during the displacement of two visco-plastic fluids. This phenomenon results when the yield stress of the displaced fluid is not exceeded at the wall of the channel, which can occur only when the yield stress of the displaced fluid is larger than that of the displacing fluid. In those displacements for which a static residual wall layer results, it has been observed that the displacement front advances steadily down the slot, leaving behind a more or less uniform layer, [3]. An example of this is given in Fig. 1a (taken from [3]), which shows the concentration profiles taken from the results of a fully two-dimensional computation at successive times. This observation of steady propagation prompts one to directly consider a steady state model, with moving coordinates fixed to the displacement front. This is the focus of this paper.

The displacement problem described above provides an idealised model for the formation of a *wet micro-annulus*, due to poor mud removal during the primary cementing of an oil well. Drilling muds, spacer fluids, and cement slurries are often visco-plastic. The static residual wall layers that we investigate correspond to layers of *gelled* or *unyielded* drilling mud that are not removed from the well during a laminar displacement. These layers are important for two reasons. Firstly, as a source of potential contamination, the mud can adversely affect the eventual mechanical properties of the cement. Secondly, after the cement has set residual wall layers of mud provide a potential channel between different fluid-bearing regions of the rock formation. The permeability of the residual mud layer is likely to be much less than that of the set cement (which is placed there to isolate the fluid-bearing zones of the formation). Any communication between zones can lower the pore pressure in the formation and have a detrimental effect on the productivity of a reservoir. As illustrated schematically in Fig. 1b, oil wells are generally long and thin, primary cementing takes place in narrow eccentric annular ducts and these ducts may be approximated locally by a plane channel (or slot). This is the underlying industrial relevance and motivation for this paper. Further details of the primary cementing process are given in [8, 13].

The main practical questions in the situation described above are, firstly to determine whether or not a static residual layer can exist, and secondly to determine its thickness. These two questions have been partially answered in [3], but many points remain unclear. In [3] a lubrication approximation was used to show that sufficient conditions for the non-existence of a static wall layer can be given in terms of two dimensionless parameters: the Bingham number for the displacing fluid (B_c) and the ratio of the yield stresses of the two fluids (φ_Y). When these conditions are not met, it is possible to compute the maximum possible static wall layer thickness h_{\max} , which depends on B_c , φ_Y , and on a third dimensionless parameter φ_B , which is a buoyancy to yield stress ratio. On computing displacements using the lubrication approximation, the interface was observed to asymptotically approach the maximum static layer thickness as $t \rightarrow \infty$. However, results from fully two-dimensional transient displacement computations (as in Fig. 1a), indicated that the static layer residual layers h were usually significantly thinner than h_{\max} . A simple explanation for this is that the fully two-dimensional flows generate larger shear stresses than the lubrication model flows. A second observation made in [3] is that the actual static layer thickness h is very close to that layer thickness at which the displaced fluid begins to recirculate ahead of the displacement front, when viewed in a frame of reference moving with the steady finger velocity. An heuristic explanation of why this should approximately select the layer thickness was given in [3], in

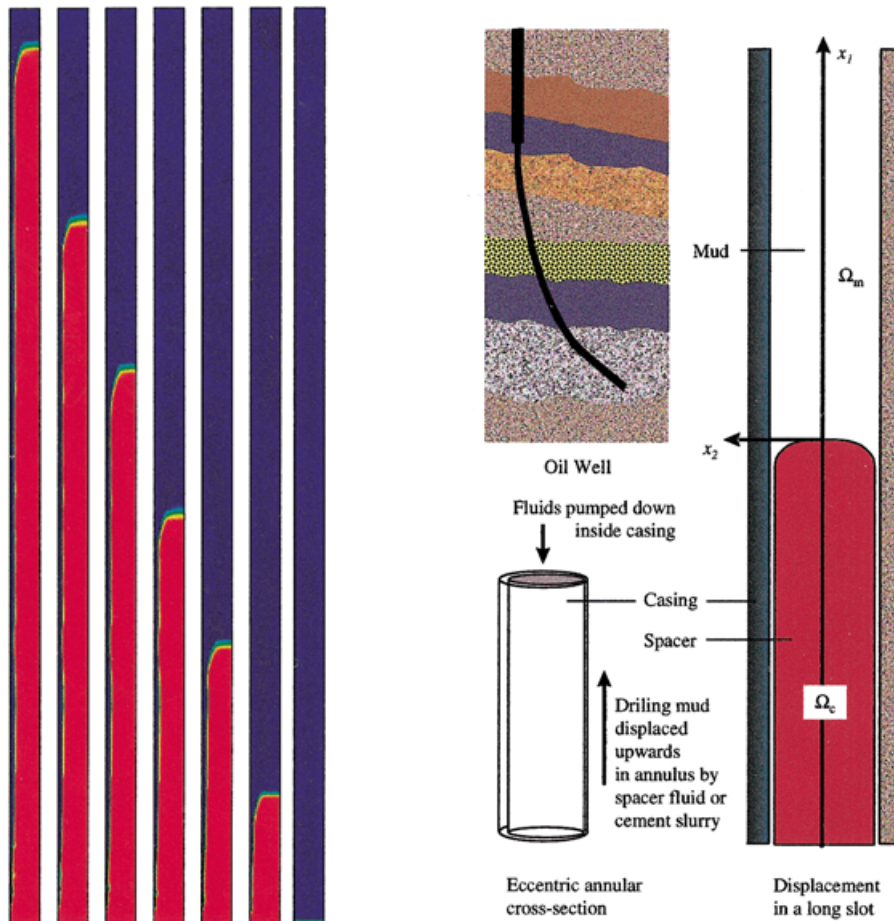


Fig. 1. a) A two-dimensional time-dependent iso-density displacement through a slot $c(x_1, x_2, t) = 1$ is red, $c(x_1, x_2, t) = 0$ is blue. Rheological parameters are $(\tau_{1,Y}, \tau_{2,Y}, \mu_1, \mu_2) = (0.2, 0.5, 0.01, 0.05)$; times (right to left): $t = 0.001, t = 3.8, t = 7.92, t = 11.7, t = 15.8, t = 20.0, t = 25.0$. b) Schematic of the industrial process of primary cementing of an oil well, illustrating the relation of eccentric annular displacements to slot displacements

terms of minimising the visco-plastic energy dissipation rate. However, exact selection of the actual layer thickness remains unclear.

The problem we have explained is one of the class of *finger width selection* problems typified by the well known Saffman-Taylor problem (see for example [11,12] or the recently studied miscible version, [10]). However, the problem considered here differs in two important respects. First, the displacements considered are not Hele-Shaw displacements. Second, the non-Newtonian nature of the fluids is wholly responsible for the phenomenon which we study, i.e. the static layer. In considering miscible displacements with Newtonian fluids in long thin geometries, but without the Hele-Shaw simplifications, the studies which are closest to ours are [4, 15], both of which investigate the high Peclet number (Pe) limit characteristic of passive scalar advection with a sharp interface. These papers are reviewed in [3] and here we mention only that similarities are few, mainly since the analogous Newtonian displacements do not exhibit properly static layers and steady states. The Saffman-Taylor fingering problem for a bubble passing through a Bingham fluid in a Hele-Shaw cell has been considered in [2] (see also the brief discussion in [14]), and shows that the fluid not displaced can be properly static between the propagating fingers. Although here we do not adopt the simplifications of the Hele-Shaw approach, the twin phenomena of static residual layers and steady finger propagation are analogous.

An outline of the paper is as follows. In § 2 we introduce the dimensionless model equations for a steady-state displacement between two Bingham fluids, in particular focusing on the boundary conditions that allow static wall layer solutions. Section 3 derives preliminary results needed for later development of the theory. We show that under suitable conditions the problem is elliptic and that for suitable rheological parameters and interface, we are able to construct a divergence free vector which satisfies all boundary and interface conditions. This allows us to homogenise the problem. The principal existence and uniqueness results are proven in § 4, using a fixed point method. Section 5 presents numerical results showing that for a wide range of finger shapes and layer thicknesses we are able to compute a solution to the steady problem. In general, we show that steady velocity solutions are computable for $h \in (h_{\min}, h_{\max})$ and the parametric variation of h_{\min} is explored.

2. Steady state displacements

Consider the steady displacement of two visco-plastic fluids in a long plane channel, i.e. a slot. The displacement is modelled as being miscible, but with a vanishingly small diffusion coefficient, i.e., the limit of infinitely large Peclet number is considered. This assumption results in the two fluid regions being separated by a sharp interface, which is formally equivalent to an immiscible displacement with insignificant surface tension. The flow is two-dimensional and steady, when viewed in a frame of reference moving with the steady speed of the displacement front, say S . We denote by fluid m the fluid that is being displaced and by fluid c the fluid that is displacing. Nominally these denote a drilling mud and a cement slurry, respectively, although the cement slurry might commonly be replaced by a visco-plastic spacer fluid. The region occupied by fluid k is denoted Ω_k . Coordinates (x_1, x_2) are fixed to the moving displacement front, such that the x_1 -axis is aligned with the slot centerline, see Fig. 1b. For simplicity, the problem is formulated with the assumption that the displacement front is symmetric with respect to the x_1 -axis. The methods and results can be extended to steady displacements that are not symmetric. Physically, the symmetry assumption is likely to be valid only in iso-density displacements or in buoyant (density-stable) displacements with the slot aligned vertically.

The dimensionless field equations for the above situation are

$$r \left[u_1 \frac{\partial u_1}{\partial x_1} + u_2 \frac{\partial u_1}{\partial x_2} \right] = -\frac{\partial p_c}{\partial x_1} + \frac{\partial}{\partial x_1} \tau_{c,11} + \frac{\partial}{\partial x_2} \tau_{c,12} - b, \quad (x_1, x_2) \in \Omega_c, \quad (1)$$

$$r \left[u_1 \frac{\partial u_2}{\partial x_1} + u_2 \frac{\partial u_2}{\partial x_2} \right] = -\frac{\partial p_c}{\partial x_2} + \frac{\partial}{\partial x_1} \tau_{c,21} + \frac{\partial}{\partial x_2} \tau_{c,22}, \quad (x_1, x_2) \in \Omega_c, \quad (2)$$

$$u_1 \frac{\partial u_1}{\partial x_1} + u_2 \frac{\partial u_1}{\partial x_2} = -\frac{\partial p_m}{\partial x_1} + \frac{\partial}{\partial x_1} \tau_{m,11} + \frac{\partial}{\partial x_2} \tau_{m,12}, \quad (x_1, x_2) \in \Omega_m, \quad (3)$$

$$u_1 \frac{\partial u_2}{\partial x_1} + u_2 \frac{\partial u_2}{\partial x_2} = -\frac{\partial p_m}{\partial x_2} + \frac{\partial}{\partial x_1} \tau_{m,21} + \frac{\partial}{\partial x_2} \tau_{m,22}, \quad (x_1, x_2) \in \Omega_m, \quad (4)$$

$$0 = \frac{\partial u_1}{\partial x_1} + \frac{\partial u_2}{\partial x_2}, \quad (x_1, x_2) \in \Omega_k, \quad k = c, m. \quad (5)$$

The velocity vector is $\mathbf{u} \equiv (u_1, u_2)$, p_k is the modified pressure, and $\tau_{k,ij}$ is the deviatoric stress tensor in fluid k . The velocity has been made dimensionless with the mean displacement velocity \tilde{U}_0 and the scaling used for the stresses is $\hat{\rho}_m \tilde{U}_0^2$, where $\hat{\rho}_m$ is the density of the displaced fluid. The pressure p_k is measured relative to the static pressure gradient of fluid m . All lengths have been scaled with the slot half-width \tilde{D} . The fluid domain is therefore $\mathbf{x} \equiv (x_1, x_2) \in (-L, L) \times (-1, 1)$, where the dimensionless length L is assumed finite, but large. The two dimensionless parameters in (1)–(5) are the density ratio and buoyancy parameter:

$$r \equiv \frac{\hat{\rho}_c}{\hat{\rho}_m} \geq 1, \quad b \equiv \frac{[\hat{\rho}_c - \hat{\rho}_m] \hat{g} \tilde{D}}{\hat{\rho}_m \tilde{U}_0^2} \geq 0. \quad (6)$$

The buoyancy parameter compares the relative importance of buoyancy and inertial stresses. Iso-density displacements correspond to the limiting values: $r = 1$ and $b = 0$. The fluids are assumed to be Bingham fluids, with constitutive laws

$$\dot{\gamma}(\mathbf{u}) = 0 \iff \tau_k(\mathbf{u}) \leq \tau_{k,Y}, \quad \mathbf{x} \in \Omega_k, \quad (7a)$$

$$\tau_{k,ij}(\mathbf{u}) = \left[\mu_k + \frac{\tau_{k,Y}}{\dot{\gamma}(\mathbf{u})} \right] \dot{\gamma}_{ij}(\mathbf{u}) \iff \tau_k(\mathbf{u}) > \tau_{k,Y}, \quad \mathbf{x} \in \Omega_k. \quad (7b)$$

The rate of strain and deviatoric stress second invariants, $\dot{\gamma}(\mathbf{u})$ and $\tau_k(\mathbf{u})$ respectively, are defined by

$$\dot{\gamma}(\mathbf{u}) = \left[\frac{1}{2} \dot{\gamma}_{ij}(\mathbf{u}) \dot{\gamma}_{ij}(\mathbf{u}) \right]^{1/2}, \quad \tau_k(\mathbf{u}) = \left[\frac{1}{2} \tau_{k,ij}(\mathbf{u}) \tau_{k,ij}(\mathbf{u}) \right]^{1/2} \quad (8)$$

where

$$\dot{\gamma}_{ij}(\mathbf{u}) = \frac{\partial u_i}{\partial x_j} + \frac{\partial u_j}{\partial x_i}, \quad (9)$$

and in (8) we have adopted the usual convention of implicitly summing over repeated coordinate indices, e.g.

$$\dot{\gamma}_{ij}(\mathbf{u}) \dot{\gamma}_{ij}(\mathbf{u}) \equiv \sum_{i,j=1}^2 [\dot{\gamma}_{ij}(\mathbf{u})]^2.$$

This convention will be used throughout the paper, except for the fluid index k , which we shall always state explicitly. The parameters in (7) are the dimensionless plastic viscosities and yield stresses:

$$\tau_{k,Y} \equiv \frac{\hat{\tau}_{k,Y}}{\hat{\rho}_m \tilde{U}_0^2}, \quad \mu_k \equiv \frac{\hat{\mu}_k}{\hat{\rho}_m \tilde{U}_0 \tilde{D}}, \quad k = c, m, \quad (10)$$

where the dimensional plastic viscosities are $\hat{\mu}_k$, $k = c, m$, and the dimensional yield stresses are $\hat{\tau}_{k,Y}$, $k = c, m$. We assume that the rheological parameters are strictly positive.

2.1 Boundary conditions

In the steadily moving frame of reference, the walls of the slot are translated in the negative x_1 -direction with the propagation speed S . Boundary conditions on the walls of the slot are given by the no-slip condition, i.e.

$$u_1(x_1, \pm 1) = -S, \quad u_2(x_1, \pm 1) = 0. \tag{11}$$

Far-field boundary conditions at $x_1 = \pm L$ are derived from one-dimensional models. These describe a steady axial flow driven by a pressure gradient. Since the mean velocity has been used as the velocity scale, the inflow and outflow velocity profiles must also satisfy an integral constraint (i.e., so that the average velocity in the non-moving frame of reference is equal to 1). The flow rate constraint is explained later, see (23). A derivation of the axial model and a discussion of the velocity profiles that we impose at the inflow is given in [3].

Downstream at $x_1 = L$, only fluid m is present. The velocity field is one-dimensional and the axial velocity component adopts the familiar profile of plane Poiseuille flow of a Bingham fluid, translated by the propagation speed S .

$$u_1(L, x_2) = U_L(x_2), \quad u_2(L, x_2) = 0, \tag{12}$$

where

$$U_L(x_2) = \begin{cases} \frac{3}{Y_{m,Y} + 2} - S, & |x_2| \in [0, Y_{m,Y}), \\ \frac{3}{Y_{m,Y} + 2} \left[1 - \frac{(|x_2| - Y_{m,Y})^2}{(1 - Y_{m,Y})^2} \right] - S, & |x_2| \in [Y_{m,Y}, 1]. \end{cases} \tag{13}$$

This function $U_L(x_2)$ consists of a parabolic segment and a constant segment. These segments join at $|x_2| = Y_{m,Y}$ which represents the positions of the yield surfaces in fluid m . The parameter $Y_{m,Y}$ is given by

$$Y_{m,Y} = \frac{1}{\xi(B_m)}, \tag{14}$$

where $B_m \equiv \tau_{m,Y}/\mu_m$ is the Bingham number for fluid m , and $\xi(B)$ is the only root of the parametric cubic equation

$$2\xi^3 - \left(3 + \frac{6}{B} \right) \xi^2 + 1 = 0, \tag{15}$$

that satisfies $\xi(B) > 1$ for $B > 0$. The function $\xi(B)$ is easily found numerically and $1/\xi(B)$ has been plotted in Fig. 2c. The Poiseuille flow profile for a Bingham fluid is derived in many introductory texts and the only notable difference here is in the scaling adopted and in the fact that (23) is satisfied, which leads to (15).

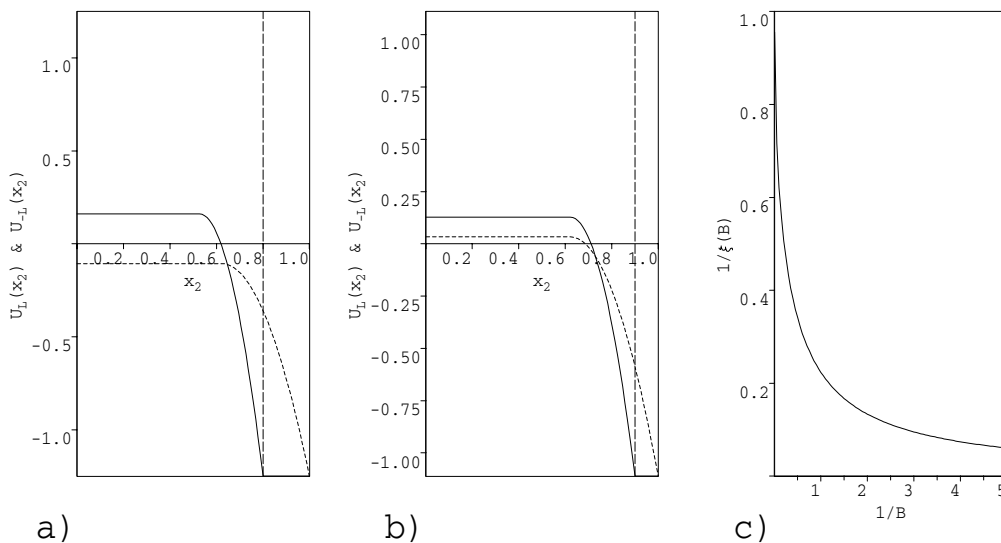


Fig. 2. Example boundary conditions $U_L(x_2)$ and $U_{-L}(x_2)$ for an iso-density displacement; rheological parameters are $(\tau_{c,Y}, \tau_{m,Y}, \mu_c, \mu_m) = (0.2, 0.5, 0.01, 0.05)$: a) propagation speed $S = 1.25$, b) propagation speed $S = 10/9$, c) the function $1/\xi(B)$ plotted against $1/B$. The dashed vertical line in a) and b) illustrates the position of the interface upstream at $x_1 = -L$

Upstream at $x_2 = -L$, the inflow profile is slightly different since there are two parallel fluid layers. We define the inflow velocity $U_{-L}(x_2)$ by

$$u_1(-L, x_2) = U_{-L}(x_2), \quad u_2(-L, x_2) = 0, \quad (16)$$

where

$$U_{-L}(x_2) = \begin{cases} \frac{3}{Y_{c,Y} + 2Y_{-L}} - S, & |x_2| \in [0, Y_{c,Y}), \\ \frac{3}{Y_{c,Y} + 2Y_{-L}} \left[1 - \frac{(|y| - Y_{c,Y})^2}{(Y_{-L} - Y_{c,Y})^2} \right] - S, & |x_2| \in [Y_{c,Y}, Y_{-L}], \\ -S, & |x_2| \in (Y_{-L}, 1]. \end{cases} \quad (17)$$

Note that the position of the interface at $x_1 = -L$ is given by $x_2 = \pm Y_{-L}$ and that the fluid for $|x_2| \in (Y_{-L}, 1]$ is moving with the (constant) speed of the wall. Thus, by *static*, in this frame of reference we mean that the fluid is fixed to the wall, i.e., it is static relative to the walls of the slot. The occurrence of axial velocity profiles of type (17) is explained fully in [3]. The positions $|x_2| = Y_{c,Y}$ in (17) are positions of the yield surfaces in fluid c , with $Y_{c,Y}$ defined by

$$Y_{c,Y} = Y_{-L}/\xi(\tilde{B}_c) \quad (18)$$

where $B_c \equiv \tau_{c,Y}/\mu_c$ is the Bingham number for fluid c and $\tilde{B}_c = B_c/S^2$.

We shall demonstrate presently that $Y_{-L} = 1/S$ in a steadily propagating displacement flow. Thus, apart from rheological constants, the boundary conditions are parameterised solely by the propagation speed S . Examples of the far-field velocity functions are illustrated in Figs. 2a and 2b for two different front propagation speeds. In both cases an iso-density displacement is considered with rheological parameters $(\tau_{c,Y}, \tau_{m,Y}, \mu_c, \mu_m) = (0.2, 0.5, 0.01, 0.05)$. Propagation speeds are $S = 5/4$ ($Y_{-L} = 0.8$) and $S = 10/9$ ($Y_{-L} = 0.9$).

2.2 Interface conditions

The interface is denoted Γ and is defined by $x_2 = \pm Y_i(x_1)$. We are interested only in steadily propagating interfaces that are both physical and that might sensibly correspond to an interface that propagates steadily along an infinitely long slot. Thus, we suppose that there exists a constant $l \in (0, L)$ such that

$$Y_i(x_1) = Y_{-L} : x_1 \in [-L, -l], \quad \forall L \gg l \text{ as } L \rightarrow \infty. \quad (19)$$

That is, we assume that the interface becomes strictly parallel to the x -axis before $x = -L$ and that this limit is independent of L as $L \rightarrow \infty$. In fact this *compactness* condition is not needed for anything that follows, but seems to be needed to extend the existence results to an infinite domain. The *static layer thickness* h is defined by

$$h \equiv 1 - Y_{-L}. \quad (20)$$

The steady state kinematic equation for the interface motion is

$$u_1 \frac{dY_i}{dx_1} = u_2 \implies \mathbf{u} \cdot \mathbf{n}_k = 0, \quad (21)$$

where $\mathbf{n}_k = (n_{k,1}, n_{k,2})$ is the outward normal vector from within Ω_k . Thus, the interface is a streamline for the steady flow. It is worth noting that if a steady miscible flow is considered (with vanishingly small diffusivity), the iso-concentration lines are also streamlines for the flow.

As remarked previously, the propagation speed S and the layer thickness h (i.e. Y_{-L}), are not independent. Integrating eq. (5) over Ω_c , using the divergence theorem and (21), implies that

$$\int_{-Y_i(x_1)}^{Y_i(x_1)} u(x_1, x_2) dy = 0. \quad (22)$$

However, due to the velocity scaling with the mean inflow velocity (in the non-moving frame of reference), we also have

$$\int_{-1}^1 [u(x_1, x_2) + S] dy = 2. \quad (23)$$

Since $u(x_1, x_2) = -S$ in the static layer, combining (22) and (23) for $x_1 < -l$ gives

$$-2S(1 - Y_{-L}) + 2S = 2 \implies Y_{-L} = \frac{1}{S}. \quad (24)$$

Thus, the static layer thickness h is fixed by the steady propagation speed S . In the sequel we shall use S , h , and Y_{-L} interchangeably. Note that with the assumption of symmetry along $x_1 = 0$, as well as (22) and (23), we also have the

conditions

$$\int_0^{\pm Y_i(x_1)} u(x_1, x_2) dy = 0, \quad \int_0^{\pm 1} [u(x_1, x_2) + S] dy = \pm 1. \tag{25}$$

The physical conditions that should be satisfied on Γ are that both components of the velocity and traction vector will be continuous across the interface. The traction vector $\boldsymbol{\sigma}_{\Gamma,k}$ is defined on each side of Γ by

$$\boldsymbol{\sigma}_{\Gamma,k} = (\sigma_{\Gamma,k,1}, \sigma_{\Gamma,k,2}) : \sigma_{\Gamma,k,i} = [-p_k \delta_{ij} + \tau_{k,ij}(\mathbf{u})] n_{k,j}, \quad k = c, m. \tag{26}$$

We denote by $[\cdot]|\Gamma$ the jump in a quantity across the interface. We have the following continuity conditions:

$$[u_i]|\Gamma = 0, \quad i = 1, 2, \tag{27}$$

$$\sigma_{\Gamma,c,i} + \sigma_{\Gamma,m,i} = 0, \quad i = 1, 2. \tag{28}$$

Apart from the physical conditions (21), (27), and (28), we wish to impose a number of restrictions on the shape of the interface. The first such restriction is (19) and we suppose that the following conditions are also satisfied by the interface parameterisation $Y_i(x)$:

$$Y_i(x_1) \in C[-L, L] \cap C^\infty[0, L] \cap C^2[-L, 0) \cap C^\infty[-L, -l], \tag{29}$$

$$Y_i'(x_1) \leq 0, \quad \forall x_1, \tag{30}$$

$$Y_i(x_1) \equiv 0 \iff x_1 \geq 0, \tag{31}$$

$$\lim_{x_1 \rightarrow 0^-} Y_i'(x_1) \neq 0, \tag{32}$$

$$Y_i(x_1) \in [Y_{c,Y}, 1/S] \implies |Y_i''(x_1)| + |Y_i'''(x_1)| < \infty. \tag{33}$$

Conditions (19) and (29)–(33) amount to saying that the interface is a smooth symmetric finger, with no cusp at $x_1 = 0$; the set Ω_c will be a smooth finger-shaped region lying in $x_1 < 0$ and touching the x_1 -axis at $x_1 = 0$. Eq. (29) is the necessary smoothness. Eqs. (19) and (29)–(31) imply that $Y_i(x_1) \in [0, Y_{-L}] \forall x_1$. Eq. (32) avoids a cusp at $x_1 = 0$ and eq. (33) states that if the interface becomes perpendicular to the x_1 axis, then it does so only for $Y_i(x_1) \in [Y_{c,Y}, 1/S]$, the meaning of which will become clear later.

3. Preliminary results

We start with some notation. For the remainder of this paper let $\Omega = (-L, L) \times (-1, 1)$, with Ω_c and Ω_m two open subsets of Ω :

$$\Omega_c \cap \Omega_m = \emptyset \quad \text{and} \quad \Omega_c \cup \Omega_m = \Omega. \tag{34}$$

The interface $\Gamma = \bar{\Omega}_c \cap \bar{\Omega}_m$ is assumed to satisfy (19) and (29)–(33). We denote the boundaries of each individual subset by $\partial\Omega_k$, $k = c, m$, and the boundary of Ω by $\partial\Omega$. We denote by $\mathbf{u}_{\partial\Omega}$ the boundary velocity function that is defined on $\partial\Omega$ by the conditions (11), (12), and (16). Let

$$\bar{H}^1(\Omega) = \left\{ \mathbf{v} = (v_1, v_2) : \frac{\partial v_i}{\partial x_j} \in L^2(\Omega), \quad i, j = 1, 2 \right\} \tag{35}$$

be the space of vector valued functions, with which we associate the semi-norm

$$\|\mathbf{v}\|_{\bar{H}^1} := \left(\int_{\Omega} \frac{\partial v_i}{\partial x_j} \frac{\partial v_i}{\partial x_j} d\Omega \right)^{1/2}. \tag{36}$$

Moreover, let

$$\mathcal{V}_0 = \{ \mathbf{v} : \mathbf{v} \in \mathcal{D}(\Omega)^2, \nabla \cdot \mathbf{v} = 0 \text{ in } \Omega, \mathbf{v} \cdot \mathbf{n} = 0 \text{ on } \Gamma, \text{ and } \mathbf{v} = 0 \text{ on } \partial\Omega \}.$$

In the above, $\mathcal{D}(\Omega)$ denotes the set of C^∞ functions with compact support on Ω . The spaces $\bar{\mathcal{V}}_0$ and $\bar{\mathcal{V}}$ are now defined by

$$\bar{\mathcal{V}}_0 = \text{closure of } \mathcal{V}_0 \text{ with respect to the norm } \|\cdot\|_{\bar{H}^1(\Omega)}, \tag{37}$$

$$\bar{\mathcal{V}} = \{ \mathbf{v} \in H^1(\Omega) : \nabla \cdot \mathbf{v} = 0 \text{ in } \Omega, \mathbf{v} \cdot \mathbf{n} = 0 \text{ on } \Gamma, \text{ and } \mathbf{v} = \mathbf{u}_{\partial\Omega} \text{ on } \partial\Omega \}. \tag{38}$$

We note that $\bar{\mathcal{V}}$ is an affine space, i.e. $\bar{\mathcal{V}} = \mathbf{u}^* + \bar{\mathcal{V}}_0$ for any $\mathbf{u}^* \in \bar{\mathcal{V}}$. A second remark is that on the interface Γ , the functions $\mathbf{v} \in \bar{\mathcal{V}}$ and $\mathbf{v}^0 \in \bar{\mathcal{V}}_0$ do not necessarily satisfy $\nabla \cdot \mathbf{v}^0 = 0$, $\nabla \cdot \mathbf{v} = 0$ pointwise. By the definition of the spaces $\bar{\mathcal{V}}_0$, $\bar{\mathcal{V}}$ this condition must hold only almost everywhere on Ω . The restrictions of a functions \mathbf{v} , \mathbf{v}^0 on Γ as well as the data at the boundary are to be understood in the sense of traces.

Now, we show that $\|\cdot\|_{\bar{H}^1}$ is a norm on $\bar{\mathcal{V}}_0$, which gives an equivalent characterisation of the space $\bar{\mathcal{V}}_0$:

$$\bar{\mathcal{V}}_0 = \text{closure of } \mathcal{V}_0 \text{ with respect to the norm } \|\cdot\|_{\bar{H}^1(\Omega)}. \tag{39}$$

Clearly $\|\cdot\|_{\bar{H}^1}$ provides a semi-norm on $\bar{\mathcal{V}}_0$. It remains to show that $\mathbf{v}^0 \equiv 0$ for any $\mathbf{v}^0 \in \bar{\mathcal{V}}_0$ satisfying $\|\mathbf{v}^0\|_{\bar{H}^1} = 0$. Let Ω^+ and Ω^- be the partitions of Ω into the sets with positive and negative x_2 components, respectively. Let $\mathbf{v}^0 \in \mathcal{V}_0$. Then, from the Cauchy-Schwarz inequality it follows that for $i = 1, 2$

$$\int_{\Omega^-} (v_i^0)^2(x_1, x_2) d\Omega = \int_{\Omega^-} \left(\int_{-1}^{x_2} \frac{\partial v_i^0}{\partial x_2}(x_1, y) dy \right)^2 d\Omega \leq \int_{\Omega^-} \int_{-1}^{x_2} \left(\frac{\partial v_i^0}{\partial x_2}(x_1, y) \right)^2 dy d\Omega \leq \int_{\Omega^-} \left(\frac{\partial v_i^0}{\partial x_2}(x_1, x_2) \right)^2 d\Omega.$$

Using the fact that $\bar{\mathcal{V}}_0$ is the closure of \mathcal{V}_0 , these arguments show that

$$\|\mathbf{v}^0\|_{L^2(\Omega)} \leq \left\| \frac{\partial \mathbf{v}^0}{\partial x_2} \right\|_{L^2(\Omega)}$$

for all $\mathbf{v}^0 \in \bar{\mathcal{V}}_0$. This shows that $\|\cdot\|_{\bar{H}^1}$ and $\|\cdot\|_{H^1}$ are equivalent norms on $\bar{\mathcal{V}}_0$, with

$$\|\cdot\|_{\bar{H}^1} \leq \|\cdot\|_{H^1} \leq \sqrt{2} \|\cdot\|_{\bar{H}^1}. \quad (40)$$

Moreover, $\bar{\mathcal{V}}_0$ associated with the inner product

$$\langle \mathbf{v}^0, \mathbf{w}^0 \rangle_{\bar{H}^1} \equiv \frac{\partial v_i^0}{\partial x_j} \frac{\partial w_i^0}{\partial x_j}$$

is a Hilbert space.

3.1 Variational formulation

The classical formulation consists of eqs. (1)–(5) and (7), with the associated boundary and interface conditions. In order to surmount potential problems associated with the interface and with computing yield surfaces in each fluid domain, a variational formulation is adopted. For $\mathbf{v}, \mathbf{u} \in \bar{\mathcal{V}}$, the following inequality is derived from the classical formulation (e.g. following the methods in [5]). The solution \mathbf{u} satisfies

$$a(\mathbf{u}, \mathbf{v} - \mathbf{u}) + b(\mathbf{u}, \mathbf{u}, \mathbf{v} - \mathbf{u}) + j(\mathbf{v}) - j(\mathbf{u}) \geq 0, \quad \mathbf{u} \in \bar{\mathcal{V}}, \quad \forall \mathbf{v} \in \bar{\mathcal{V}}, \quad (41)$$

where

$$a(\mathbf{v}, \mathbf{w}) \equiv \left\{ \frac{\mu_c}{2} \int_{\Omega_c} \dot{\gamma}_{ij}(\mathbf{v}) \dot{\gamma}_{ij}(\mathbf{w}) d\Omega + \frac{\mu_m}{2} \int_{\Omega_m} \dot{\gamma}_{ij}(\mathbf{v}) \dot{\gamma}_{ij}(\mathbf{w}) d\Omega \right\}, \quad \forall \mathbf{v}, \mathbf{w} \in \bar{\mathcal{V}} \text{ or } \bar{\mathcal{V}}_0, \quad (42)$$

$$b(\mathbf{u}, \mathbf{v}, \mathbf{w}) \equiv \left\{ r \int_{\Omega_c} u_j \frac{\partial v_i}{\partial x_j} w_i d\Omega + \int_{\Omega_m} u_j \frac{\partial v_i}{\partial x_j} w_i d\Omega \right\}, \quad \forall \mathbf{u}, \mathbf{v}, \mathbf{w} \in \bar{\mathcal{V}} \text{ or } \bar{\mathcal{V}}_0, \quad (43)$$

$$j(\mathbf{v}) \equiv \tau_{c,Y} \int_{\Omega_c} \dot{\gamma}(\mathbf{v}) d\Omega + \tau_{m,Y} \int_{\Omega_m} \dot{\gamma}(\mathbf{v}) d\Omega, \quad \forall \mathbf{v} \in \bar{\mathcal{V}} \text{ or } \bar{\mathcal{V}}_0. \quad (44)$$

The derivation of (41) is as follows. We take the scalar product of (1)–(4) with $\mathbf{v} - \mathbf{u}$, integrate over the different fluid domains and sum to give

$$b(\mathbf{u}, \mathbf{u}, \mathbf{v} - \mathbf{u}) = \sum_{k=c,m} \int_{\Omega_k} \frac{\partial}{\partial x_j} ([v_i - u_i] [-p_k \delta_{ij} + \tau_{k,ij}(\mathbf{u})]) - \frac{1}{2} \dot{\gamma}_{ij}(\mathbf{v} - \mathbf{u}) \tau_{k,ij}(\mathbf{u}) d\Omega - b \int_{\Omega_c} [v_1 - u_1] d\Omega. \quad (45)$$

Letting \mathbf{n}_k denote the outward normal to Ω_k , the first term on the right-hand side of (45) transforms via Green's theorem into

$$\sum_{k=c,m} \int_{\partial\Omega_k} [v_i - u_i] [-p_k \delta_{ij} + \tau_{k,ij}(\mathbf{u})] n_{k,j} ds = \sum_{k=c,m} \int_{\Gamma} [v_i - u_i] [\sigma_{\Gamma,c,i} + \sigma_{\Gamma,m,i}] ds = 0 \quad (46)$$

since $v_i - u_i$ vanishes on the walls, inflow and outflow, and the interface integral cancels between the two domains, using (27)–(28). The last term in (45) vanishes using (22), which must also hold for $\mathbf{v} \in \bar{\mathcal{V}}$. For the remaining term, the inequality

$$\frac{1}{2} \dot{\gamma}_{ij}(\mathbf{v} - \mathbf{u}) \tau_{k,ij}(\mathbf{u}) = \mu_k \frac{1}{2} \dot{\gamma}_{ij}(\mathbf{v} - \mathbf{u}) \dot{\gamma}_{ij}(\mathbf{u}) + \tau_{k,Y} \left[\frac{1}{2} \frac{\dot{\gamma}_{ij}(\mathbf{v}) \dot{\gamma}_{ij}(\mathbf{u})}{\dot{\gamma}(\mathbf{u})} - \dot{\gamma}(\mathbf{u}) \right] \quad (47)$$

$$\leq \mu_k \frac{1}{2} \dot{\gamma}_{ij}(\mathbf{v} - \mathbf{u}) \dot{\gamma}_{ij}(\mathbf{u}) + \tau_{k,Y} [\dot{\gamma}(\mathbf{v}) - \dot{\gamma}(\mathbf{u})] \quad (48)$$

follows from the Cauchy-Schwarz inequality when $\dot{\gamma}(\mathbf{u}) > 0$, and trivially when $\dot{\gamma}(\mathbf{u}) = 0$ since then we have $\tau_k(\mathbf{u}) \leq \tau_{k,Y}$ and again apply the Cauchy-Schwarz inequality. Therefore, eventually

$$0 = b(\mathbf{u}, \mathbf{u}, \mathbf{v} - \mathbf{u}) + \sum_{k=c,m} \int_{\Omega_k} \frac{1}{2} \dot{\gamma}_{ij}(\mathbf{v} - \mathbf{u}) \tau_{k,ij}(\mathbf{u}) \, d\Omega \leq a(\mathbf{u}, \mathbf{v} - \mathbf{u}) + b(\mathbf{u}, \mathbf{u}, \mathbf{v} - \mathbf{u}) + j(\mathbf{v}) - j(\mathbf{u}). \tag{49}$$

3.1.1 Properties of $a(\cdot, \cdot)$

We are primarily interested in the continuity and ellipticity of the bilinear form $a(\cdot, \cdot)$. From the definition of $a(\cdot, \cdot)$ it follows that

$$a(\mathbf{v}, \mathbf{w}) \leq \max\{\mu_k\} \int_{\Omega} \frac{1}{2} |\dot{\gamma}_{ij}(\mathbf{v}) \dot{\gamma}_{ij}(\mathbf{w})| \, d\Omega \leq 8 \max\{\mu_k\} \|\mathbf{v}\|_{\bar{H}_1} \|\mathbf{w}\|_{\bar{H}_1}. \tag{51}$$

For the ellipticity of $a(\cdot, \cdot)$ on the space $\bar{\mathcal{V}}_0$, we first note that

$$a(\mathbf{u}, \mathbf{u}) \geq \min\{\mu_k\} \sum_{k=c,m} \int_{\Omega_k} \frac{1}{2} \dot{\gamma}_{ij}(\mathbf{u}) \dot{\gamma}_{ij}(\mathbf{u}) \, d\Omega.$$

For the sake of simplicity, let $\mathbf{u} \in \{C^2(\bar{\Omega}_c) \times C^2(\bar{\Omega}_m)\} \cap \bar{\mathcal{V}}_0$, then we have

$$\sum_{k=c,m} \int_{\Omega_k} \frac{1}{2} \dot{\gamma}_{ij}(\mathbf{u}) \dot{\gamma}_{ij}(\mathbf{u}) \, d\Omega = \sum_{k=c,m} \int_{\Omega_k} \left[\frac{\partial u_i}{\partial x_j} \right] \left[\frac{\partial u_i}{\partial x_j} \right] + \left[\frac{\partial u_i}{\partial x_j} \right] \left[\frac{\partial u_j}{\partial x_i} \right] \, d\Omega. \tag{52}$$

We show that the second term on the right-hand side above vanishes. Let Ω_k^+ be the subset of Ω_k with positive x_2 and Ω_k^- the subset of Ω_k with negative x_2 . We consider first Ω_c^+ and use Green's theorem in the plane:

$$\int_{\Omega_c^+} \frac{\partial u_i}{\partial x_j} \frac{\partial u_j}{\partial x_i} \, d\Omega = \int_{\Omega_c^+} \frac{\partial}{\partial x_i} \left[u_j \frac{\partial u_i}{\partial x_j} \right] \, d\Omega \tag{53}$$

$$= \int_{-L}^0 \left[u_1 \frac{\partial u_2}{\partial x_1} + u_2 \frac{\partial u_2}{\partial x_2} - \frac{dY_i}{dx_1} \left(u_1 \frac{\partial u_1}{\partial x_1} + u_2 \frac{\partial u_1}{\partial x_2} \right) \right]_{(x_1, x_2)=(x_1, Y_i(x_1))} \, dx_1. \tag{54}$$

Now we use the identity $\mathbf{u} \cdot \mathbf{n} = 0$ to write

$$u_2 = \frac{dY_i}{dx_1} u_1, \tag{55}$$

and we differentiate the identity $\mathbf{u} \cdot \mathbf{n} = 0$, with respect to x_1 , to give

$$0 = \frac{d}{dx_1} u_2(x_1, Y_i(x_1)) - \frac{dY_i}{dx_1} \frac{d}{dx_1} u_1(x_1, Y_i(x_1)) - u_1(x_1, Y_i(x_1)) \frac{d^2 Y_i}{dx_1^2}, \tag{56}$$

where d/dx_1 denotes the total derivative with respect to x_1 , and where in both (55) and (56) the limits in approaching the interface are taken from within Ω_c^+ . Combining these, we get

$$\int_{\Omega_c^+} \frac{\partial u_i}{\partial x_j} \frac{\partial u_j}{\partial x_i} \, d\Omega = \int_{-L}^0 u_1 \left[\frac{\partial u_2}{\partial x_1} + \frac{dY_i}{dx_1} \frac{\partial u_2}{\partial x_2} - \frac{dY_i}{dx_1} \left(\frac{\partial u_1}{\partial x_1} + \frac{dY_i}{dx_1} \frac{\partial u_1}{\partial x_2} \right) \right]_{(x_1, x_2)=(x_1, Y_i(x_1))} \, dx_1 \tag{57}$$

$$= \int_{-L}^0 \left[u_1 u_1 \frac{d^2 Y_i}{dx_1^2} \right]_{(x_1, x_2)=(x_1, Y_i(x_1))} \, dx_1. \tag{58}$$

Now we integrate over Ω_m^+ :

$$\int_{\Omega_m^+} \frac{\partial u_i}{\partial x_j} \frac{\partial u_j}{\partial x_i} \, d\Omega = \int_{\Omega_m^+} \frac{\partial}{\partial x_i} \left[u_j \frac{\partial u_i}{\partial x_j} \right] \, d\Omega \tag{59}$$

$$= - \int_{-L}^0 \left[u_1 \frac{\partial u_2}{\partial x_1} + u_2 \frac{\partial u_2}{\partial x_2} - \frac{dY_i}{dx_1} \left(u_1 \frac{\partial u_1}{\partial x_1} + u_2 \frac{\partial u_1}{\partial x_2} \right) \right]_{(x_1, x_2)=(x_1, Y_i(x_1))} \, dx_1 \tag{60}$$

$$= - \int_{-L}^0 u_1 \left[\frac{\partial u_2}{\partial x_1} + \frac{dY_i}{dx_1} \frac{\partial u_2}{\partial x_2} - \frac{dY_i}{dx_1} \left(\frac{\partial u_1}{\partial x_1} + \frac{dY_i}{dx_1} \frac{\partial u_1}{\partial x_2} \right) \right]_{(x_1, x_2)=(x_1, Y_i(x_1))} \, dx_1 \tag{61}$$

$$= - \int_{-L}^0 \left[u_1 u_1 \frac{d^2 Y_i}{dx_1^2} \right]_{(x_1, x_2)=(x_1, Y_i(x_1))} \, dx_1, \tag{62}$$

where we have again used the identities (55) and (56), but have now evaluated the limits by approaching the interface from within Ω_m^+ . Thus, on summing (58) and (62), the boundary integrals cancel. The same is true for the integrals over Ω_c^- and Ω_m^- . The following lemma is an immediate consequence of the above considerations.

Lemma 1: *The bilinear form $a(\cdot, \cdot)$ is continuous on $\bar{\mathcal{V}} \times \bar{\mathcal{V}}_0 \cup \bar{\mathcal{V}}_0 \times \bar{\mathcal{V}}$ and for all $\mathbf{u}, \mathbf{v} \in \bar{\mathcal{V}}$*

$$|a(\mathbf{u}, \mathbf{v})| \leq 8 \max\{\mu_k\} \|\mathbf{u}\|_{\bar{H}^1} \|\mathbf{v}\|_{\bar{H}^1}. \quad (63)$$

The bilinear form $a(\cdot, \cdot)$ is relative elliptic on $\bar{\mathcal{V}}_0$, i.e., for all $\mathbf{u} \in \bar{\mathcal{V}}_0$

$$\min\{\mu_k\} \|\mathbf{u}\|_{\bar{H}^1}^2 \leq a(\mathbf{u}, \mathbf{u}). \quad (64)$$

3.1.2 Properties of $b(\cdot, \cdot, \cdot)$

We consider the trilinear form $b(\cdot, \cdot, \cdot)$ on $\bar{\mathcal{V}} \times \bar{\mathcal{V}} \times \bar{\mathcal{V}}$ (or any other combination of $\bar{\mathcal{V}}$ and $\bar{\mathcal{V}}_0$).

Lemma 2: *For all $\mathbf{u}, \mathbf{v}, \mathbf{w} \in \bar{\mathcal{V}}$ or $\bar{\mathcal{V}}_0$, the trilinear form $b(\cdot, \cdot, \cdot)$ satisfies*

$$|b(\mathbf{u}, \mathbf{v}, \mathbf{w})| \leq C_b \|\mathbf{u}\|_{H^1} \|\mathbf{v}\|_{H^1} \|\mathbf{w}\|_{H^1}. \quad (65)$$

The trilinear form $b(\cdot, \cdot, \cdot)$ satisfies

$$b(\mathbf{v}, \mathbf{w}, \mathbf{w}) = 0, \quad (66)$$

for any of the following cases: (i) $\mathbf{v} \in \bar{\mathcal{V}}$ and $\mathbf{w} \in \bar{\mathcal{V}}_0$; (ii) $\mathbf{w} \in \bar{\mathcal{V}}$ and $\mathbf{v} \in \bar{\mathcal{V}}_0$; (iii) $\mathbf{v}, \mathbf{w} \in \bar{\mathcal{V}}_0$.

The trilinear form $b(\cdot, \cdot, \cdot)$ satisfies

$$b(\mathbf{u}, \mathbf{v}, \mathbf{w}) = -b(\mathbf{u}, \mathbf{w}, \mathbf{v}), \quad (67)$$

for any of the following cases: (i) $\mathbf{u} \in \bar{\mathcal{V}}$ and $\mathbf{v}, \mathbf{w} \in \bar{\mathcal{V}}_0$; (ii) $\mathbf{v}, \mathbf{w} \in \bar{\mathcal{V}}$ and $\mathbf{u} \in \bar{\mathcal{V}}_0$; (iii) $\mathbf{u}, \mathbf{v}, \mathbf{w} \in \bar{\mathcal{V}}_0$.

Proof: From the Cauchy Schwarz inequality it follows that

$$\left| \int_{\Omega_k} u_j \frac{\partial v_j}{\partial x_i} w_j \, d\Omega \right| \leq \|u_j\|_{L^4(\Omega_k)} \|v_j\|_{\bar{H}^1(\Omega_k)} \|w_j\|_{L^4(\Omega_k)}.$$

Now, we use a Sobolev embedding theorem (see e.g. [1]) which states that

$$\|\cdot\|_{L^4(\Omega_k)} \leq C_S \|\cdot\|_{H^1(\Omega_k)}. \quad (68)$$

This shows (65). For property (67), integrating by parts and using the divergence theorem gives

$$b(\mathbf{u}, \mathbf{v}, \mathbf{w}) = \left\{ r \int_{\partial\Omega_c} [u_j v_i w_i n_{c,j}] \, ds + \int_{\partial\Omega_m} [u_j v_i w_i n_{m,j}] \, ds \right\} - b(\mathbf{u}, \mathbf{w}, \mathbf{v}).$$

The surface integrals vanish in the cases specified. Property (66) follows immediately from (67). \square

Lemma 3: *Let $\mathbf{u}_n \in \bar{\mathcal{V}}_0$ converge weakly to \mathbf{u}^+ with respect to the \bar{H}^1 -norm. Then for any $\mathbf{v} \in \bar{\mathcal{V}}$,*

$$b(\mathbf{u}_n, \mathbf{u}_n, \mathbf{v}) \rightarrow b(\mathbf{u}^+, \mathbf{u}^+, \mathbf{v}), \quad b(\mathbf{v}, \mathbf{u}_n, \mathbf{u}_n) \rightarrow b(\mathbf{v}, \mathbf{u}^+, \mathbf{u}^+), \quad \text{and} \quad b(\mathbf{u}_n, \mathbf{v}, \mathbf{u}_n) \rightarrow b(\mathbf{u}^+, \mathbf{v}, \mathbf{u}^+).$$

Proof: We use the Rellich-Kandrchov compact embedding theorem (see [1]) which in particular states that the embedding of H^1 into L^4 is compact. Let $\{\mathbf{u}_n\}$ be a sequence, which is weakly convergent to \mathbf{u}^+ with respect to the H^1 -norm. Then from standard results on weak convergence it follows that $\|\mathbf{u}_n\|_{H^1}$ is uniformly bounded. From the compactness of the embedding of H^1 into L^4 we can deduce the existence of a subsequence \mathbf{u}_k , which is strongly convergent to \mathbf{u}^+ in L^4 . Thus

$$|b(\mathbf{u}_k, \mathbf{u}_k, \mathbf{v}) - b(\mathbf{u}^+, \mathbf{u}^+, \mathbf{v})| \leq r \sum_{k=c,m} \left| \int_{\Omega_k} (u_{n,j} - u_j^+) \frac{\partial u_{n,i}}{\partial x_j} v_i \right| + r \sum_{k=c,m} \left| \int_{\Omega_k} u_j^+ \left(\frac{\partial u_{n,i}}{\partial x_j} - \frac{\partial u_i^+}{\partial x_j} \right) v_i \right|. \quad (69)$$

Using Sobolev's embedding theorem (cf. (68)) it follows that the first term of the sum on the right hand side can be estimated by $C_S \|u_{n,j} - u_j^+\|_{L^4} \|u_{n,i}\|_{\bar{H}^1} \|v_i\|_{L^4}$, which converges to zero as k tends to infinity. To prove that the second term tends to zero, too, we apply Green's formula and get

$$\int_{\Omega_k} u_j^+ \left(\frac{\partial u_{n,i}}{\partial x_j} - \frac{\partial u_i^+}{\partial x_j} \right) v_i = - \int_{\Omega_k} \frac{\partial u_j^+}{\partial x_j} (u_{n,i} - u_i^+) v_i - \int_{\Omega_k} \frac{\partial v_i}{\partial x_j} (u_{n,i} - u_i^+) u_j + \int_{\partial\Omega_k} v_i (u_{n,i} - u_i^+) u_j^+ n_j.$$

Since $\mathbf{u} \in \bar{\mathcal{V}}$ and $\mathbf{v} \in \bar{\mathcal{V}}_0$, the boundary integral vanishes. The absolute value of the first integral on the right hand side of the above identity can be estimated by $\|u_j\|_{\bar{H}^1} \|u_{n,i} - u_i\|_{L^4} \|v_i\|_{L^4}$, which tends to zero for $n \rightarrow \infty$. Moreover, the second term can be estimated by $\|u_j\|_{L^4} \|u_{n,i} - u_i\|_{L^4} \|v_i\|_{\bar{H}^1}$, which tends to zero, too. The other convergence results are proven similarly. \square

3.1.3 Properties of $j(\cdot)$

We verify that the functional $j(\cdot)$ is continuous on $\bar{\mathcal{V}}$ with respect to the H^1 -norm.

Lemma 4: For all $\mathbf{u}^0, \mathbf{v}^0 \in \bar{\mathcal{V}}_0, \mathbf{u}^* \in \bar{\mathcal{V}}$

$$|j(\mathbf{u}^* + \mathbf{u}^0) - j(\mathbf{u}^* + \mathbf{v}^0)| \leq C_j \|\mathbf{u}^0 - \mathbf{v}^0\|_{H^1}. \tag{70}$$

Proof: We denote $\mathbf{u} = \mathbf{u}^* + \mathbf{u}^0$ and $\mathbf{v} = \mathbf{u}^* + \mathbf{v}^0$. Using the Cauchy-Schwartz inequality,

$$\begin{aligned} |j(\mathbf{u}) - j(\mathbf{v})| &= \sum_{k=c,m} \left\{ \tau_{k,Y} \left| \int_{\Omega_k} \dot{\gamma}(\mathbf{u}) - \dot{\gamma}(\mathbf{v}) \, d\Omega \right| \right\} = \sum_{k=c,m} \left\{ \tau_{k,Y} \left| \int_{\Omega_k} \frac{\dot{\gamma}^2(\mathbf{u}) - \dot{\gamma}^2(\mathbf{v})}{\dot{\gamma}(\mathbf{u}) + \dot{\gamma}(\mathbf{v})} \, d\Omega \right| \right\} \\ &= \sum_{k=c,m} \left\{ \tau_{k,Y} \left| \int_{\Omega_k} \frac{\frac{1}{2} \dot{\gamma}_{ij}(\mathbf{u}_0 - \mathbf{v}_0) \dot{\gamma}_{ij}(\mathbf{u} + \mathbf{v})}{\dot{\gamma}(\mathbf{u}) + \dot{\gamma}(\mathbf{v})} \, d\Omega \right| \right\} \leq \sum_{k=c,m} \left\{ \tau_{k,Y} \int_{\Omega_k} \frac{\dot{\gamma}(\mathbf{u}_0 - \mathbf{v}_0) \dot{\gamma}(\mathbf{u} + \mathbf{v})}{\dot{\gamma}(\mathbf{u}) + \dot{\gamma}(\mathbf{v})} \, d\Omega \right\} \\ &\leq \sum_{k=c,m} \left\{ \tau_{k,Y} \int_{\Omega_k} \dot{\gamma}(\mathbf{u}_0 - \mathbf{v}_0) \, d\Omega \right\} \leq \max\{\tau_{k,Y}\} \sqrt{\text{meas}(\Omega)} \left[\int_{\Omega} \dot{\gamma}^2(\mathbf{u}_0 - \mathbf{v}_0) \, d\Omega \right]^{1/2} \\ &\leq \max\{\tau_{k,Y}\} \sqrt{\text{meas}(\Omega)} \|\mathbf{u}^0 - \mathbf{v}^0\|_{H^1} \end{aligned}$$

which shows that (70) holds with $C_j = \max\{\tau_{k,Y}\} \sqrt{\text{meas}(\Omega)}$. □

3.2 Homogenisation of the variational problem

It is more convenient to consider the test space $\bar{\mathcal{V}}_0$ rather than $\bar{\mathcal{V}}$. Thus, we homogenise (41) by constructing $\mathbf{u}^* \in \bar{\mathcal{V}}$. This construction has some implications for the type of interface which can be considered; see § 3.2.1. Here precisely, we look for a function $\mathbf{u}^* = (u_1^*, u_2^*) \in \bar{\mathcal{V}}$ such that

$$u_1^*(x_1, x_2) = g(x_1) U_{-L}(x_2) + [1 - g(x_1)] U_L(x_2), \tag{71}$$

where $g(x_1)$ satisfies the following far-field conditions:

$$g(x_1) \rightarrow 1, \quad g'(x_1) \rightarrow 0, \quad \text{for } x_1 \rightarrow -l, \tag{72}$$

$$g(x_1) \rightarrow 0, \quad g'(x_1) \rightarrow 0, \quad \text{for } x_1 \rightarrow l. \tag{73}$$

Recall that $l < L$ describes the limit at which the interface is assumed to become parallel to the x -axis, upstream. The condition $\nabla \cdot \mathbf{u}^* = 0$ is satisfied if

$$u_2^*(x_1, x_2) = - \int_0^{x_2} \frac{\partial u^*}{\partial x_1}(x_1, \tilde{x}_2) \, d\tilde{x}_2 = g'(x_1) [\Psi_L(x_2) - \Psi_{-L}(x_2)], \tag{74}$$

where $\Psi_L(x_2)$ and $\Psi_{-L}(x_2)$ are the far-field stream-functions, defined by

$$\Psi_L(x_2) \equiv \int_0^{x_2} U_L(\tilde{x}_2) \, d\tilde{x}_2, \quad \Psi_{-L}(x_2) \equiv \int_0^{x_2} U_{-L}(\tilde{x}_2) \, d\tilde{x}_2. \tag{75}$$

From (71), (72), and (73) it is clear that $u_1^*(x_1, x_2)$ satisfies the boundary conditions for u_1 in (11), (12), and (16), both for $x_1 = \pm L$ and for $x_2 = \pm 1$. It is a matter of simple algebra to verify that $\Psi_L(\pm 1) = \Psi_{-L}(\pm 1)$, so that from (72), (73), and (74) it is evident that the boundary conditions for u_2 in (11), (12), and (16) are also satisfied, i.e.

$$\mathbf{u}^* = \mathbf{u}_{\partial\Omega} \quad \text{on } \partial\Omega.$$

We note that \mathbf{u}^* is symmetric about the x_1 -axis. For the remainder, to simplify algebra we confine our attention only to $x_2 \geq 0$; the extension to $x_2 \leq 0$ by symmetry, being straightforward. For a given interface $\Gamma: x_2 = Y_i(x_1)$, we denote by $A(x_1)$ the function

$$A(x_1) \equiv \int_0^{Y_i(x_1)} [U_{-L}(\tilde{x}_2) - U_L(\tilde{x}_2)] \, d\tilde{x}_2 = \Psi_{-L}(Y_i(x_1)) - \Psi_L(Y_i(x_1)).$$

In order for $\mathbf{u}^* \cdot \mathbf{n} = 0$ to be satisfied on Γ , we require that

$$A'(x_1) g(x_1) + Y_i'(x_1) U_L(Y_i(x_1)) + g'(x_1) A(x_1) = 0,$$

which can be written as

$$\frac{d}{dx_1} [A(x_1) g(x_1) + \Psi_L(Y_i(x_1))] = 0. \tag{76}$$

Using (25) and (72), this equation is integrated from $x_1 = -L$ to finally define $g(x_1)$ by

$$g(x_1) = -\frac{\Psi_L(Y_i(x_1))}{A(x_1)} = \frac{\Psi_L(Y_i(x_1))}{\Psi_L(Y_i(x_1)) - \Psi_{-L}(Y_i(x_1))}. \quad (77)$$

Note that (77) depends only on x_1 only through $Y_i(x_1)$. We define

$$G(x_2) \equiv \frac{\Psi_L(x_2)}{\Psi_L(x_2) - \Psi_{-L}(x_2)} \quad (78)$$

and suppose that

$$U_{-L}(0) - U_L(0) > 0. \quad (79)$$

We have the following subsidiary result on the properties of $G(x_2)$.

Lemma 5: *Suppose $S > 1$ and that (79) is satisfied. Then $G(x_2) \in C^2[0, 1/S] \cap C^1[0, 1]$.*

Proof: The proof is in five stages:

(i) Condition (79) with the definitions (13) and (17) implies that

$$Y_{m,Y} - Y_{c,Y} > 2(1/S - 1) > 0.$$

Thus, for $x_2 \in [0, Y_{c,Y}]$,

$$\Psi_L(x_2) - \Psi_{-L}(x_2) = [U_L(0) - U_{-L}(0)] x_2 < 0, \quad x_2 \in [0, Y_{c,Y}],$$

$$G(x_2) = \frac{U_L(0)}{U_L(0) - U_{-L}(0)} = \text{const.}, \quad x_2 \in [0, Y_{c,Y}].$$

Therefore, for $x_2 \in [0, Y_{c,Y}]$, we even have $G(x_2) \in C^\infty$.

(ii) We note that $U_L(x_2) \in C^1[0, 1]$ and $U_{-L}(x_2) \in C[0, 1] \cap C^1[0, 1/S] \cap C^\infty[1/S, 0]$. Thus, $\Psi_L(x_2)$ and $\Psi_{-L}(x_2)$ have the necessary smoothness; the proof requires only that

$$\Psi_L(x_2) - \Psi_{-L}(x_2) < 0, \quad x_2 \in [Y_{c,Y}, 1]. \quad (80)$$

(iii) From definitions (13) and (17), $U_{-L}(x_2) - U_L(x_2) < 0$ for $x_2 \in [1/S, 1]$, and since $\Psi_L(1) - \Psi_{-L}(1) = 0$,

$$\Psi_L(x_2) - \Psi_{-L}(x_2) = \int_{x_2}^1 [U_{-L}(\tilde{x}_2) - U_L(\tilde{x}_2)] d\tilde{x}_2 < 0, \quad x_2 \in [1/S, 1].$$

(iv) Thus, $\Psi_L(x_2) - \Psi_{-L}(x_2) < 0$ at both endpoints of the interval $[Y_{c,Y}, 1/S]$. Furthermore, $\Psi_L(x_2) - \Psi_{-L}(x_2)$ is C^1 on $[0, 1]$; strictly decreasing at $x_2 = Y_{c,Y}$ and strictly increasing at $x_2 = 1/S$. Necessary condition for there to be a zero of $\Psi_L(x_2) - \Psi_{-L}(x_2)$ in $[Y_{c,Y}, 1/S]$ is that

$$\frac{d}{dx_2} [\Psi_L - \Psi_{-L}] \equiv U_L(x_2) - U_{-L}(x_2) = 0, \quad (81)$$

has three solutions in $[Y_{c,Y}, 1/S]$.

(v) Since $U_L(Y_{c,Y}) - U_{-L}(Y_{c,Y}) < 0$ and $U_L(1/S) - U_{-L}(1/S) > 0$, eq. (81) has at least one solution. For (81) to have three solutions would require that

$$\frac{d}{dx_2} [U_L(x_2) - U_{-L}(x_2)] = 0 \quad (82)$$

has three solutions on $[Y_{c,Y}, 1/S]$. However, for $x_2 \in [Y_{c,Y}, Y_{M,Y})$, the function $U_L(x_2) - U_{-L}(x_2)$ is strictly increasing and for $x_2 \in [Y_{M,Y}, 1/S)$, the function $U_L(x_2) - U_{-L}(x_2)$ is linear. Consequently, (82) can have at most one solution, (81) has only one solution, and (80) holds.

3.2.1 Restrictions on $Y_i(x_1)$

We would like to find conditions such that the first partial derivatives of \mathbf{u}^* exist pointwise on Ω_c and Ω_m . In the above construction of \mathbf{u}^* , there are few restrictions made on $g(x_1)$ for $x_1 > 0$. At $x_1 = 0$, we have that

$$g(0) = \frac{U_L(0)}{U_L(0) - U_{-L}(0)},$$

and all that is required is that $g(x_1)$ be twice continuously differentiable across $x_1 = 0$ and $g(x_1) \in C^2[0, L]$, with the limit conditions (73) satisfied. The choice of $g(x_1): x_1 \in [0, L]$ is therefore fairly arbitrary. It is worth noting that if we take any such suitable $g(x_1)$ in the definitions (71) and (74), the partial derivatives of \mathbf{u}^* are continuous everywhere

for $x_1 \in [0, L]$, except on the line $x_2 = 1/S$. The problem at $x_2 = 1/S$ is only with

$$\frac{\partial u^*}{\partial x_2}(x_1, x_2) = U'_L(x_2) + g(x_1) [U'_L(x_2) - U'_{-L}(x_2)],$$

which will have a discontinuity across $x_2 = 1/S$, due to the discontinuity in $U'_{-L}(x_2)$ across $x_2 = 1/S$. However, at least $\nabla \cdot \mathbf{u}^* = 0$ pointwise for $x_1 \in [0, L]$.

Considering now $x_1 \in [-L, 0]$, from the definitions (71) and (74), we see that

$$\frac{\partial u^*}{\partial x_1}(x_1, x_2) = -Y'_i(x_1) G'(Y_i(x_1)) [U_L(x_2) - U_{-L}(x_2)], \tag{83}$$

$$\frac{\partial u^*}{\partial x_2}(x_1, x_2) = U'_L(x_2) + G(Y_i(x_1)) [U'_L(x_2) - U'_{-L}(x_2)], \tag{84}$$

$$\frac{\partial v^*}{\partial x_1}(x_1, x_2) = [Y''_i(x_1) G'(Y_i(x_1)) + [Y'_i(x_1)]^2 G''(Y_i(x_1))] [\Psi_L(x_2) - \Psi_{-L}(x_2)], \tag{85}$$

$$\frac{\partial v^*}{\partial x_2}(x_1, x_2) = Y'_i(x_1) G'(Y_i(x_1)) [U_L(x_2) - U_{-L}(x_2)]. \tag{86}$$

In Lemma 5 we have shown that $G(x_2)$ is C^2 for $x_2 \in [0, 1/S]$. Conditions (19) and (29)–(33) are assumed to be satisfied by the interfaces under consideration. Note that (19) and (29)–(31) are sufficient for the partial derivatives of \mathbf{u}^* to exist pointwise in each of Ω_c and Ω_m , except potentially at $x_1 = 0$. Eq. (33) ensures that when the interface approaches the x_1 -axis perpendicularly then it can only become perpendicular to the x_1 -axis for $x_2 < Y_{c,Y}$. The significance of this is that for $x_2 < Y_{c,Y}$, assuming the conditions of Lemma 5, $G(x_2)$ is constant and consequently \mathbf{u}^* is also constant in this range of x_1 (i.e. this range of $Y_i(x_1)$). Therefore, conditions (19) and (29)–(33) are sufficient for the partial derivatives of \mathbf{u}^* to exist pointwise in each of Ω_c and Ω_m for $x_1 \in [-L, 0]$. Indeed, the partial derivatives of \mathbf{u}^* will be continuous everywhere except across $x_2 = 1/S$ where there is a jump discontinuity in (84), due to the discontinuity in $U'_{-L}(x_2)$ across $x_2 = 1/S$. In particular $\nabla \cdot \mathbf{u}^* = 0$ pointwise for $x_1 \in [-L, 0]$ and hence throughout Ω_c and Ω_m . We have proven the following result.

Lemma 6: *Suppose $S > 1$, that (79) is satisfied by the far-field velocities and that the interface satisfies (19)–(33). Then there exists $\mathbf{u}^* = (u^*, v^*) \in \bar{\mathcal{V}}$, that can be constructed by (71), (74) with $g(x_1)$ defined by (77).*

4. Existence and uniqueness results

In § 3.2 we have shown by construction that there exists $\mathbf{u}^* \in \bar{\mathcal{V}}$. We use this to homogenise the inequality (41). We write the solution to (41), $\mathbf{u} \in \bar{\mathcal{V}}$ and also arbitrary $\mathbf{v} \in \bar{\mathcal{V}}$ as follows:

$$\mathbf{u} = \mathbf{u}^* + \mathbf{u}^0 \quad \text{and} \quad \mathbf{v} = \mathbf{u}^* + \mathbf{v}^0,$$

where $\mathbf{u}^0, \mathbf{v}^0 \in \bar{\mathcal{V}}_0$. In place of (41) we will consider

$$\tilde{a}(\mathbf{u}^0, \mathbf{v}^0 - \mathbf{u}^0) + b(\mathbf{u}^0, \mathbf{u}^0, \mathbf{v}^0) + j(\mathbf{u}^* + \mathbf{v}^0) - j(\mathbf{u}^* + \mathbf{u}^0) \geq L(\mathbf{v}^0 - \mathbf{u}^0), \quad \mathbf{u}^0 \in \bar{\mathcal{V}}_0, \quad \forall \mathbf{v}^0 \in \bar{\mathcal{V}}_0, \tag{87}$$

where

$$\tilde{a}(\mathbf{v}^0, \mathbf{w}^0) \equiv a(\mathbf{v}^0, \mathbf{w}^0) + b(\mathbf{u}^*, \mathbf{v}^0, \mathbf{w}^0) + b(\mathbf{v}^0, \mathbf{u}^*, \mathbf{w}^0), \tag{88}$$

$$L(\mathbf{v}^0) \equiv -a(\mathbf{u}^*, \mathbf{v}^0) - b(\mathbf{u}^*, \mathbf{u}^*, \mathbf{v}^0). \tag{89}$$

More formally, since $a(\mathbf{v}^0, \mathbf{w}^0)$, $b(\mathbf{u}^*, \mathbf{v}^0, \mathbf{w}^0)$, and $b(\mathbf{v}^0, \mathbf{u}^*, \mathbf{w}^0)$ are continuous bilinear forms on $\bar{\mathcal{V}}_0$ (in \mathbf{v}^0 and \mathbf{w}^0), it follows from the Riesz representation theorem that there exist operators A, B_c, B_m which satisfy

$$\langle A\mathbf{v}^0, \mathbf{w}^0 \rangle_{H^1} = a(\mathbf{v}^0, \mathbf{w}^0),$$

$$\langle B_c\mathbf{v}^0, \mathbf{w}^0 \rangle_{H^1} = b(\mathbf{v}^0, \mathbf{u}^*, \mathbf{w}^0),$$

$$\langle B_m\mathbf{v}^0, \mathbf{w}^0 \rangle_{H^1} = b(\mathbf{u}^*, \mathbf{w}^0, \mathbf{v}^0).$$

We introduce the operator $\tilde{A} = A + B_c + B_m$ and the associated bilinear form

$$\langle \tilde{A}\mathbf{v}^0, \mathbf{w}^0 \rangle_{H^1} = \tilde{a}(\mathbf{v}^0, \mathbf{w}^0) \equiv a(\mathbf{v}^0, \mathbf{w}^0) + b(\mathbf{v}^0, \mathbf{u}^*, \mathbf{w}^0) + b(\mathbf{u}^*, \mathbf{v}^0, \mathbf{w}^0).$$

For all $\mathbf{v}^0 \in \bar{\mathcal{V}}_0$, $\mathbf{v}^* \in \bar{\mathcal{V}}$ it follows that

$$(\min\{\mu_k\} - 2C_b\|\mathbf{v}^*\|_{H^1}) \|\mathbf{v}^0\|_{H^1}^2 \leq a(\mathbf{v}^0, \mathbf{v}^0) - |b(\mathbf{v}^0, \mathbf{v}^*, \mathbf{v}^0)| - |b(\mathbf{v}^*, \mathbf{v}^0, \mathbf{v}^0)| \tag{90}$$

(note that $|b(\mathbf{v}^*, \mathbf{v}^0, \mathbf{v}^0)| = 0$). In the following we assume that

$$\alpha = \min\{\mu_k\} - 2C_b \|\mathbf{u}^*\|_{H^1} > 0 \quad (91)$$

which is a condition on the plastic viscosities μ_k , i.e., that they be sufficiently large. From (63) and (65) it follows that for all $\mathbf{v}^0 \in \bar{\mathcal{V}}_0$

$$|a(\mathbf{u}^*, \mathbf{v}^0)| \leq 8 \max\{\mu_k\} \|\mathbf{u}^*\|_{\bar{H}^1} \|\mathbf{v}^0\|_{\bar{H}^1} \quad \text{and} \quad |b(\mathbf{u}^*, \mathbf{u}^*, \mathbf{v}^0)| \leq \sqrt{2} C_b \|\mathbf{u}^*\|_{H^1} \|\mathbf{u}^*\|_{H^1} \|\mathbf{v}^0\|_{\bar{H}^1},$$

which shows that $L(\mathbf{v}^0)$, defined on $\bar{\mathcal{V}}_0$, is bounded and satisfies

$$\|L\| \leq (8 \max\{\mu_k\} + \sqrt{2} C_b \|\mathbf{u}^*\|_{H^1}) \|\mathbf{u}^*\|_{H^1}. \quad (92)$$

From (87) (taking $\mathbf{v}^0 = 0$), on using (70), (90), (91), and (92) it follows that

$$\alpha \|\mathbf{u}^0\|_{\bar{H}^1}^2 \leq \tilde{a}(\mathbf{u}^0, \mathbf{u}^0) \leq L(\mathbf{v}^0) + j(\mathbf{u}^*) - j(\mathbf{u}^* + \mathbf{u}^0) \leq (\|L\| + C_j \sqrt{2}) \|\mathbf{u}^0\|_{\bar{H}^1}.$$

Therefore,

$$\|\mathbf{u}^0\|_{\bar{H}^1} \leq \frac{\|L\| + C_j \sqrt{2}}{\alpha} \equiv R. \quad (93)$$

For $\xi \in \bar{\mathcal{V}}_0$ let

$$\tilde{L}_\xi(\mathbf{v}^0) \equiv b(\xi, \xi, \mathbf{v}^0).$$

Note that \tilde{L}_ξ is a linear operator on $\bar{\mathcal{V}}_0$ and satisfies

$$\|\tilde{L}_\xi\| \leq C_b \sqrt{2} \|\xi\|_{H^1}^2.$$

Let $\xi \in \bar{\mathcal{V}}_0 \cap B_{\tilde{R}}$ be fixed and let ρ, \tilde{R} be given positive numbers. Then we consider the auxiliary problem of solving the following inequality for $\mathbf{w}^0 \in \bar{\mathcal{V}}_0$:

$$\langle \mathbf{w}^0, \mathbf{v}^0 - \mathbf{w}^0 \rangle_{H^1} + \rho [j(\mathbf{u}^* + \mathbf{v}^0) - j(\mathbf{u}^* + \mathbf{w}^0)] \geq -\rho(\tilde{L}_\xi - L)(\mathbf{v}^0 - \mathbf{w}^0) + \langle \xi, \mathbf{v}^0 - \mathbf{w}^0 \rangle_{H^1} - \rho \tilde{a}(\xi, \mathbf{v}^0 - \mathbf{w}^0), \quad (94)$$

$$\mathbf{w}^0 \in \bar{\mathcal{V}}_0, \quad \forall \mathbf{v}^0 \in \bar{\mathcal{V}}_0.$$

For arbitrary $\xi \in \bar{\mathcal{V}}_0 \cap B_{\tilde{R}}$ this inequality has a solution $\mathbf{w}^0 \in \bar{\mathcal{V}}_0$ (cf. Theorem 4.1 in [7]). We denote by \mathcal{F} the mapping from $\xi \in \bar{\mathcal{V}}_0 \cap B_{\tilde{R}}$ to the solution of (94).

Lemma 7: For ρ sufficiently small and $\alpha > 4 \sqrt{2} C_b \tilde{R}$, the mapping \mathcal{F} is a contraction.

Proof: Let $\xi_1 \neq \xi_2 \in \bar{\mathcal{V}}_0 \cap B_{\tilde{R}}$, and denote by \mathbf{w}_1^0 and \mathbf{w}_2^0 the corresponding solutions of the variation inequality (94), then

$$\begin{aligned} & \langle \mathbf{w}_1^0, \mathbf{w}_2^0 - \mathbf{w}_1^0 \rangle_{H^1} + \rho [j(\mathbf{u}^* + \mathbf{w}_2^0) - j(\mathbf{u}^* + \mathbf{w}_1^0)] \\ & \geq -\rho(\tilde{L}_{\xi_1} - L)(\mathbf{w}_2^0 - \mathbf{w}_1^0) + \langle \xi_1, \mathbf{w}_2^0 - \mathbf{w}_1^0 \rangle_{H^1} - \rho \tilde{a}(\xi_1, \mathbf{w}_2^0 - \mathbf{w}_1^0), \\ & \langle \mathbf{w}_2^0, \mathbf{w}_1^0 - \mathbf{w}_2^0 \rangle_{H^1} + \rho [j(\mathbf{u}^* + \mathbf{w}_1^0) - j(\mathbf{u}^* + \mathbf{w}_2^0)] \\ & \geq -\rho(\tilde{L}_{\xi_2} - L)(\mathbf{w}_1^0 - \mathbf{w}_2^0) + \langle \xi_2, \mathbf{w}_1^0 - \mathbf{w}_2^0 \rangle_{H^1} - \rho \tilde{a}(\xi_2, \mathbf{w}_1^0 - \mathbf{w}_2^0). \end{aligned}$$

Taking the sum of both inequalities gives

$$\|\mathbf{w}_1^0 - \mathbf{w}_2^0\|_{H^1}^2 \leq \rho \|\tilde{L}_{\xi_2} - \tilde{L}_{\xi_1}\| \|\mathbf{w}_1^0 - \mathbf{w}_2^0\|_{H^1} + \|(I - \rho \tilde{A})(\xi_2 - \xi_1)\|_{H^1} \|\mathbf{w}_1^0 - \mathbf{w}_2^0\|_{H^1},$$

and therefore

$$\|\mathbf{w}_1^0 - \mathbf{w}_2^0\|_{H^1} \leq 2\rho C_b \sqrt{2} \max\{\|\xi_1\|_{H^1}, \|\xi_2\|_{H^1}\} \|\xi_2 - \xi_1\|_{H^1} + \|(I - \rho \tilde{A})(\xi_2 - \xi_1)\|_{H^1}. \quad (95)$$

Now we take ρ to satisfy

$$0 < \rho \leq \alpha / \|\tilde{A}\|^2, \quad (96)$$

giving

$$\|I - \rho \tilde{A}\|^2 \leq 1 - 2\rho\alpha + \rho^2 \|\tilde{A}\|^2 \leq 1 - \rho\alpha \leq (1 - \rho\alpha/2)^2,$$

and eventually, since $\tilde{R} > \max\{\|\xi_1\|_{H^1}, \|\xi_2\|_{H^1}\}$

$$\|\mathbf{w}_1^0 - \mathbf{w}_2^0\|_{H^1} \leq \left(1 - \frac{\rho\alpha}{2} + 2\rho C_b \sqrt{2} \tilde{R}\right) \|\xi_1 - \xi_2\|_{H^1}, \quad (97)$$

which is obviously a contraction if $\alpha > 4C_b \sqrt{2} \tilde{R}$. \square

Theorem 8: *If $\alpha > 32 \sqrt{2} C_b R$, then the mapping \mathcal{F} which maps a function $\xi \in \bar{\mathcal{V}}_0$ onto the solution w^0 of the variational inequality (94) has a fixed point. The fixed point is the unique solution of (87).*

Proof: We take $\xi_0 = 0$ and $\xi_n := \mathcal{F}(\xi_{n-1})$. Then it follows from (94), by putting $v^0 = 0$ and $\xi = 0$, that

$$\|\xi_1\|_{H^1} \leq \rho(C_j + \|L\|) < \rho\alpha R.$$

Thus for sufficiently small ρ we have $\|\xi_1\|_{H^1} \leq 4R$. Now, we show by induction that $\|\xi_{n+1}\|_{H^1} \leq 4R$. Assuming $\|\xi_n\|_{H^1} \leq 4R$ and using (97)

$$\begin{aligned} \|\xi_{n+1}\|_{H^1} &= \|\xi_{n+1} - \xi_1 + \xi_1\|_{H^1} \leq \|\xi_{n+1} - \xi_1\|_{H^1} + \|\xi_1\|_{H^1} \leq \left(1 - \frac{\rho\alpha}{2} + 8\rho \sqrt{2} C_b R\right) \|\xi_n - \xi_0\|_{H^1} + \|\xi_1\|_{H^1} \\ &\leq \left(1 - \frac{\rho\alpha}{2} + 8\rho \sqrt{2} C_b R\right) 4R + \|\xi_1\|_{H^1} \leq \left(1 - \frac{\rho\alpha}{4} + 8\rho \sqrt{2} C_b R\right) 4R, \end{aligned}$$

which shows that $\|\xi_{n+1}\|_{H^1} \leq 4R$ under the condition $\alpha > 32C_b R$. This shows that ξ_n is uniformly bounded in H^1 , and thus it has a weakly convergent subsequence ξ_k in $\bar{\mathcal{V}}_0$. We denote the weak limit by ξ . Now, we show that ξ_n is strongly convergent to ξ . From the weak lower semicontinuity of the norm it follows that for all $n \in \mathbb{N}$

$$\|\xi_n - \xi\|_{H^1} \leq 4R \left(1 - \frac{\rho\alpha}{4} + 8\rho \sqrt{2} C_b R\right)^n. \tag{98}$$

Thus ξ_n converges strongly to ξ . From the definition of ξ_{n+1} it follows that

$$\begin{aligned} &\langle \xi_{n+1}, v^0 - \xi_{n+1} \rangle_{H^1} + \rho[j(u^* + v^0) - j(u^* + \xi_{n+1})] \\ &\geq -\rho(\tilde{L}_{\xi_n} - L)(v^0 - \xi_{n+1}) + \langle \xi_n, v^0 - \xi_{n+1} \rangle_{H^1} - \rho\tilde{a}(\xi_n, v^0 - \xi_{n+1}). \end{aligned}$$

Since $\xi_n \rightarrow \xi$ in H^1 and $L_\xi(\xi) = 0$, we get

$$\tilde{a}(\xi, v^0 - \xi) + b(\xi^0, \xi^0, v^0) + j(u^* + v^0) - j(u^* + \xi) \geq L(v^0 - \xi). \tag{99}$$

Thus we have shown that ξ is a solution of (87), which is also a fixed point of the mapping \mathcal{F} .

For uniqueness, we suppose that (87) has two solutions u_1^0 and u_2^0 , then

$$\begin{aligned} \tilde{a}(u_1^0, u_2^0 - u_1^0) + b(u_1^0, u_1^0, u_2^0) + j(u^* + u_2^0) - j(u^* + u_1^0) &\geq L(u_2^0 - u_1^0), \\ \tilde{a}(u_2^0, u_1^0 - u_2^0) + b(u_2^0, u_2^0, u_1^0) + j(u^* + u_1^0) - j(u^* + u_2^0) &\geq L(u_1^0 - u_2^0), \end{aligned}$$

and on summing

$$\tilde{a}(u_2^0 - u_1^0, u_2^0 - u_1^0) - b(u_1^0, u_1^0, u_2^0) - b(u_2^0, u_2^0, u_1^0) \leq 0. \tag{100}$$

Now, using Lemma 2,

$$\begin{aligned} b(u_1^0, u_1^0, u_2^0) + b(u_2^0, u_2^0, u_1^0) &= [b(u_1^0, u_1^0, u_2^0) - b(u_1^0, u_2^0, u_2^0) + b(u_1^0, u_2^0, u_1^0) - b(u_1^0, u_1^0, u_1^0)] \\ &\quad + [b(u_2^0, u_2^0, u_1^0) + b(u_1^0, u_2^0, u_2^0) - b(u_1^0, u_2^0, u_1^0) - b(u_2^0, u_2^0, u_2^0)] \\ &= -b(u_1^0, u_2^0 - u_1^0, u_2^0 - u_1^0) - b(u_2^0 - u_1^0, u_2^0, u_2^0 - u_1^0) \\ &= -b(u_2^0 - u_1^0, u_2^0, u_2^0 - u_1^0). \end{aligned}$$

Therefore,

$$\begin{aligned} (\alpha - C_b \sqrt{2} R) \|u_2^0 - u_1^0\|_{H^1}^2 &\leq \tilde{a}(u_2^0 - u_1^0, u_2^0 - u_1^0) - |b(u_1^0, u_2^0 - u_1^0, u_2^0 - u_1^0)| - |b(u_2^0 - u_1^0, u_2^0, u_2^0 - u_1^0)| \\ &\leq \tilde{a}(u_2^0 - u_1^0, u_2^0 - u_1^0) + b(u_1^0, u_2^0 - u_1^0, u_2^0 - u_1^0) + b(u_2^0 - u_1^0, u_2^0, u_2^0 - u_1^0) \leq 0. \end{aligned} \quad \square$$

Remark 1: Actually we have a stronger estimate than (95):

$$\|w_1^0 - w_2^0\|_{H^1} \leq 2C\rho \max\{\|\xi_2\|_{H^1}, \|\xi_1\|_{H^1}\} \|\xi_2 - \xi_1\|_{L^4} + \|(I - \rho\tilde{A})(\xi_2 - \xi_1)\|_{H^1},$$

with a generic constant C . Since the embedding of H^1 into L^4 is compact, the inequality (95) may be very crude in practical applications.

Remark 2: We note that the condition $\alpha > 32 \sqrt{2} C_b R$ is satisfied if

$$(\min\{\mu_k\} - 2C_b \|u^*\|_{H^1})^2 > 32C_b \sqrt{2} (C_j \sqrt{2} + (\max\{\mu_k\} + \sqrt{2} C_b \|u^*\|_{H^1}) \|u^*\|_{H^1}). \tag{101}$$

This condition is satisfied if the plastic viscosities are large enough, but is also significantly harder to satisfy if the plastic viscosities differ too much.

Remark 3: We note that for $L = \infty$ the above result cannot be proven using identical arguments. The main difficulty arises from the fact that in this situation the functional b is not well-defined on \bar{H}^1 . Under the assumptions

already made on the interface, the space \bar{H}^1 is a Hilbert space, but may contain elements which are not in L^2 . Actually \bar{H}^1 is a Hilbert space of functions with quadratically integrable derivatives on $(-\infty, \infty) \times (-1, 1)$ and on each compact set the function is in H^1 .

5. Limiting static layer thicknesses and example results

The main theoretical result of the paper is theorem 8, which shows that there exists a unique velocity solution to (87) for rheological parameters that render the problem sufficiently *elliptic* (see the conditions of theorem 8). Theorem 8 will also imply a unique solution to (41) if the conditions of lemmas 5 and 6 can be satisfied. Sufficient conditions for there to exist a unique solution to the steady problem are therefore

$$\alpha > 32 \sqrt{2} C_b R, \quad (102)$$

conditions (19) and (29)–(33) on the shape and smoothness of the interface and condition (79). A further necessary condition for a static wall layer solution is to be able to define the upstream velocity $U_{-L}(x_2)$ with a static layer. Necessary conditions on the far-field velocity $U_{-L}(x_2)$ for there to be a static layer of the type described above are that

$$h \in (0, h_{\max}), \quad (103)$$

where $h_{\max} \geq 0$ is the *maximum static layer thickness*. That there should exist a maximum possible static layer thickness is perfectly intuitive. According to our choice of scaling, the total areal flow rate passing through $x_2 \in [0, 1]$ is unity. However, when there is a static wall layer, the unit flow rate must pass through $x_2 \in [0, 1 - h]$. The variation in shear stress is linear in both fluids, with the maximum shear stress found at the wall. As h increases, a progressively larger axial pressure gradient is needed to produce the same flow rate through a progressively smaller gap. The shear stress increases with the axial pressure gradient and eventually the stress at the wall exceeds the finite yield stress of fluid m and the wall layer is no longer static. The maximum static layer thickness h_{\max} has been defined and computed in [3], which we do not repeat here. In short, the thickness h_{\max} depends parametrically on the fluid c Bingham number, $B_c \equiv \tau_{c,Y}/\mu_c$, on the yield stress ratio, $\varphi_Y \equiv \tau_{c,Y}/\tau_{m,Y}$, and on the buoyancy to yield ratio, $\varphi_B \equiv b/\tau_{m,Y}$. It is shown in [3] that $\varphi_Y < 1$ is a necessary condition for $h_{\max} > 0$. Examples of the variation in h_{\max} with φ_Y for different B_c and for an iso-density displacement ($\varphi_B = 0$) are plotted in Fig. 3a.

Hence, sufficient conditions for the existence of a unique solution to the steady problem with a static wall layer are: conditions (19) and (29)–(33) on the shape and smoothness of the interface, condition (79), condition (102), and condition (103). We note that the condition (102) is very unlikely to be sharp. Moreover, conditions (19) and (29)–(33) place no constraints on the fluid rheologies and leave a broad range of potential interface configurations. Thus, provided that interfaces do not contravene (79) and (103), we can reasonably expect a unique solution to the

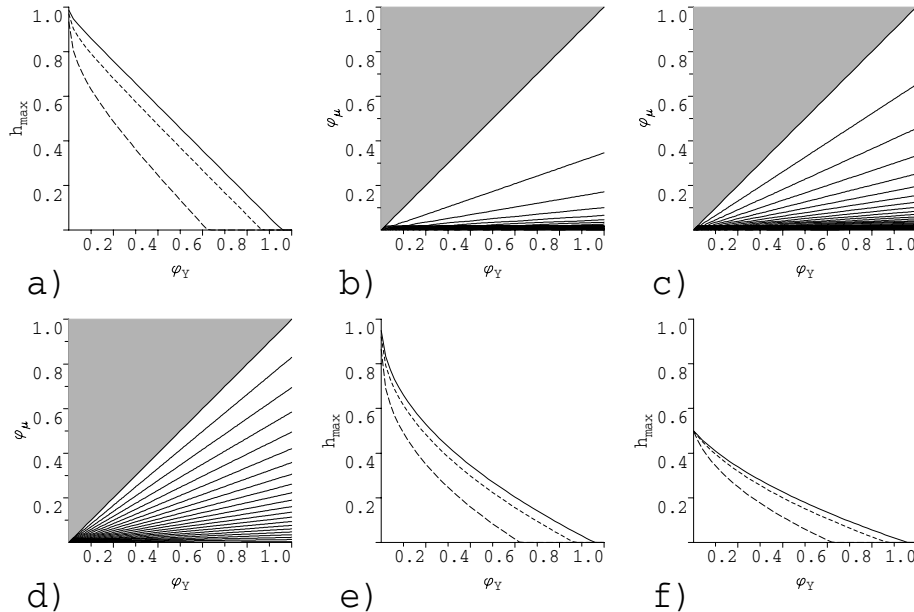


Fig. 3. Maximal and minimal static wall layers, $h_{\min} = 0$ in shaded regions. a) h_{\max} for $\varphi_B = 0.0$ for $B_c = 1000$ (solid), $B_c = 100$, $B_c = 10$; b) h_{\min} for $B_c = 1000$: contours are $\Delta h = 0.01$; c) h_{\min} for $B_c = 100$: contours are $\Delta h = 0.01$; d) h_{\min} for $B_c = 10$: contours are $\Delta h = 0.01$; e) h_{\max} for $\varphi_B = 1.0$ for $B_c = 1000$ (solid), $B_c = 100$, $B_c = 10$; f) h_{\max} for $\varphi_B = 2.0$ for $B_c = 1000$ (solid), $B_c = 100$, $B_c = 10$

steady state interface propagation problem posed in § 2, at least in a weak sense (i.e. for each fixed interface). Thus the result follows: uniqueness of solution but non-uniqueness of interface, as is commonly found for steady multi-fluid flows, see e.g. [9] for a discussion.

For practical purposes, we are not particularly interested in the exact shape of the interface, but only in possible limitations to there being a static layer thickness. The first constraint on the static layer thickness comes from (103), which is well understood: if $h > h_{\max}$ a solution may still exist, but the wall layer cannot be static. The second constraint comes from (79), which we now show is also a constraint on the static layer thickness h . If we define $F(B_c, B_m, Y_{-L})$ by

$$F(B_c, B_m, Y_{-L}) \equiv \frac{1}{Y_{m,Y} + 2} - \frac{1}{Y_{c,Y} + 2Y_{-L}}, \tag{104}$$

we see from (13) and (17) that $F(B_c, B_m, Y_{-L}) = [U_L(0) - U_{-L}(0)]/3$ and that (79) corresponds to $F(B_c, B_m, Y_{-L}) < 0$. The dependency of $F(B_c, B_m, Y_{-L})$ on B_c , B_m , and Y_{-L} is defined in § 2.1. Differentiating with respect to Y_{-L} ,

$$\frac{\partial}{\partial Y_{-L}} Y_{c,Y} = \frac{1}{\xi(\tilde{B}_c)} + Y_{-L} \frac{\partial}{\partial Y_{-L}} \left[\frac{1}{\xi(\tilde{B}_c)} \right] = \frac{1}{\xi(\tilde{B}_c)} - \frac{2}{\xi(\tilde{B}_c)} \frac{d\xi}{d\tilde{B}}(\tilde{B}_c) > 0, \tag{105}$$

implying that

$$\frac{\partial}{\partial Y_{-L}} F(B_c, B_m, Y_{-L}) > 0. \tag{106}$$

We note also that $F(B_c, B_m, Y_{-L}) \rightarrow -\infty$ as $Y_{-L} \rightarrow 0$. Therefore, we have the following two possibilities:

1. If $F(B_c, B_m, 1) < 0$ then $F(B_c, B_m, Y_{-L}) < 0, \forall Y_{-L} \in [0, 1]$. In this case there is no restriction on the layer thickness h .
2. If $F(B_c, B_m, 1) > 0$ then there exists exactly one solution to $F(B_c, B_m, Y_{-L}) = 0$ for $Y_{-L} \in (0, 1)$. We define the minimum layer thickness h_{\min} via

$$F(B_c, B_m, 1 - h_{\min}) = 0. \tag{107}$$

Note that condition (79) is satisfied only for $h > h_{\min}$.

The critical condition is $F(B_c, B_m, 1) = 1$, and it is easily seen that

$$F(B_c, B_m, 1) = 0 \iff B_c = B_m. \tag{108}$$

Eq. (107) is confined to $B_c > B_m$ and we define $h_{\min} = 0$ if $B_c \leq B_m$.

The above is a mathematical derivation of h_{\min} , the physical meaning of which will become clearer only after the computation of some numerical examples. Before this however, we are able to compare parametric variations in h_{\min} with those in h_{\max} . To this end we write

$$B_m \equiv \frac{\tau_{m,Y}}{\mu_m} = \frac{\tau_{m,Y}}{\tau_{c,Y}} \frac{\tau_{c,Y}}{\mu_c} \frac{\mu_c}{\mu_m} \equiv \varphi_\mu \frac{B_c}{\varphi_Y}, \tag{109}$$

where φ_μ is the ratio of plastic viscosities: $\varphi_\mu \equiv \mu_c/\mu_m$. For fixed B_c , the condition (108) is given by $\varphi_\mu = \varphi_Y$. For different fixed values of B_c , the variation in h_{\min} with φ_Y and φ_μ is plotted in Figs. 3b–3d. These can be compared directly with the variations in h_{\max} from Fig. 3a. Whilst in general $h_{\max} > h_{\min}$, it is clear that for sufficiently small values of φ_μ and sufficiently large values of φ_Y , the condition $h_{\max} < h_{\min}$ can also be attained. This parameter regime is that in which the displacing fluid becomes progressively *plastic* by comparison with the displaced fluid, i.e., the ratio B_m/B_c is small. The (φ_μ, φ_Y) -parameter space, in which $h_{\max} < h_{\min}$ is possible also appears to become progressively large as B_c decreases, due to the decrease in h_{\max} , which appears slightly contradictory. Note however, that a decrease in B_c for fixed yield stress $\tau_{c,Y}$ corresponds to an increase in μ_c , increasing the shear stress throughout the flow and reducing h_{\max} . In general, the conditions defining h_{\max} and h_{\min} come from completely different physical considerations and it is not surprising that these conditions are not more closely coupled. The definition of h_{\min} does not depend on the buoyancy-yield stress ratio $\varphi_B = b/\tau_{m,Y}$, but that of h_{\max} does. Fig. 3e and Fig. 3f plot the variations in h_{\max} that correspond to two different values of φ_B . Increasing φ_B reduces h_{\max} and therefore increases the (φ_μ, φ_Y) -parameter space in which $h_{\max} < h_{\min}$.

Still unclear is whether the condition $h > h_{\min}(B_c, B_m)$ is necessary as well as sufficient for there to exist a steady state solution and if so, what is happening physically as $h \rightarrow h_{\min}(B_c, B_m)$. To this end, we have computed velocity solutions for fixed rheological parameters, $(\tau_{c,Y}, \tau_{m,Y}, \mu_c, \mu_m) = (0.2, 0.5, 0.01, 0.05)$, and for different h . The flow is assumed to be iso-density. These computations have been carried out with $\Omega: (x_1, x_2) \in (0, 1) \times (-10, 10)$, with symmetry conditions imposed along $x_2 = 0$. The interface is chosen parallel to the x_1 -axis at the inflow and perpendicular to the x_1 -axis at $x_1 = 0$, joined by the (discretised) arc of a circle of radius $Y_{-L}/2$, between $(x_1, x_2) = (-Y_{-L}/2, Y_{-L})$ and $(x_1, x_2) = (0, Y_{-L}/2)$. A finite element method is used with linear basis functions on quadrilateral elements. An example mesh is shown in Fig. 4a, for $h = 0.35$. In place of the exact Bingham fluid constitutive equations, we have used a

regularised viscosity model. Eq. (7) is replaced by

$$\tau_{k,ij}(\mathbf{u}) = \eta_k(\mathbf{u}) \dot{\gamma}_{ij}(\mathbf{u}), \quad \mathbf{x} \in \Omega_k, \quad (110a)$$

$$\eta_k(\mathbf{u}) = \mu_k + \frac{\tau_{k,Y}}{\epsilon + \dot{\gamma}(\mathbf{u})}, \quad \mathbf{x} \in \Omega_k, \quad (110b)$$

where $\epsilon \ll 1$ is a regularisation parameter, fixed at $\epsilon = 10^{-3}$ for the computations presented. Use of this type of viscosity model has become fairly standard for computing viscoplastic fluid flows, although it is also not problem-free. For the chosen rheological parameters, $h_{\min} \approx 0.0323$ and $h_{\max} \approx 0.3364$. We have computed velocity solutions for different h and the streamlines for the velocity solutions are shown in Figs. 4 and 5. The stream function Ψ is defined here by

$$\Psi(x_1, x_2) = \int_{(0,0)}^{(x_1, x_2)} u(\tilde{x}_1, \tilde{x}_2) dx_2 - v(\tilde{x}_1, \tilde{x}_2) dx_1. \quad (111)$$

Only a part of Ω close to the displacement front $x_1 = 0$ is shown. The computations were carried out using the computational fluid dynamics code FIDAP, version 8.01; see [6]. This code is quite flexible, allowing the different viscosity functions $\eta_k(\mathbf{u})$ to be defined on each Ω_k by means of user-defined subroutines, likewise the far-field boundary conditions (13) and (17), and the condition $\mathbf{u} \cdot \mathbf{n} = 0$ can also be specified on the interface. Convergence usually takes somewhere between 30–60 iterations.

Figs. 4b–4f show the streamlines for layer thicknesses $h \geq 0.15$. The interface is given by the streamline $\Psi = 0$ and indeed, in Figs. 4b–4f, the line $\Psi = 0$ follows the interface fairly well. Even though we don't manage to get the line $\Psi = 0$ to intersect the x_1 -axis at $x_1 = 0$, adjacent streamlines do remain in the different fluid domains. We are reasonably satisfied that it is purely due to numerical error that we do not get the separating streamline to intercept the x_1 -axis. It should be noted that a primitive variable formulation has been used in the computation, whereas perhaps a stream function-vorticity formulation would have been preferable for this flow feature. Qualitatively, the streamlines in fluid c recirculate in Ω_c , whilst those in fluid m enter Ω_m upstream and exit through the static layer, after flowing around Ω_c . We remark that $h > h_{\max}$ in Fig. 4b, whereas $h < h_{\max}$ in Figs. 4c–4f. This computation $h = 0.35$ has been included to illustrate that steady solutions do exist for $h > h_{\max}$. There is no noticeable qualitative difference in the streamlines between Fig. 4b and Figs. 4c–4f, i.e., the parametric variation in streamline behaviour across $h = h_{\max}$ is smooth. It is simply that, for $h = 0.35$, it is not possible to impose the upstream boundary velocity profile with a static wall layer.

At smaller layer thicknesses than those shown in Fig. 4, fluid m begins to recirculate in Ω_m . The value of h at which recirculation starts is denoted h_{circ} and can be easily computed from a knowledge of the far-field downstream boundary condition, (13). For these rheological parameters, $h_{\text{circ}} \approx 0.1258$. Although not clear in Fig. 5b, there is in

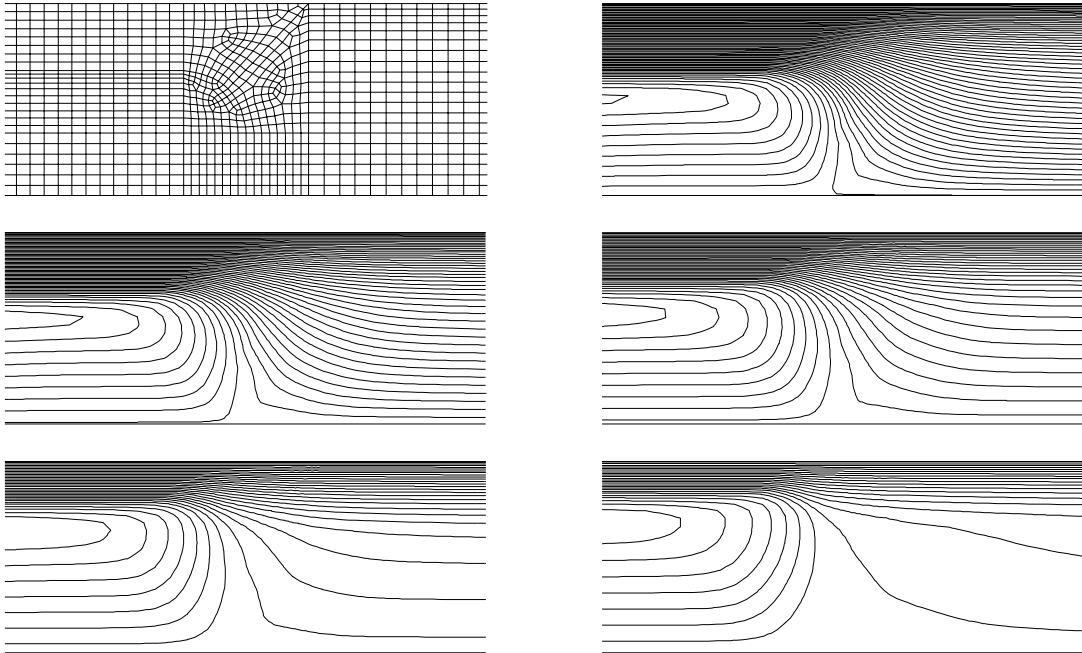


Fig. 4. Example computations for $(\tau_{c,Y}, \tau_{m,Y}, \mu_c, \mu_m) = (0.2, 0.5, 0.01, 0.05)$, showing the streamlines of the solution for different interface positions (left to right; top to bottom): a) $Y_{-L} = 1/S = 0.65$, example of finite element mesh; b) $Y_{-L} = 1/S = 0.65$, contours $\Delta\Psi = 0.01$; c) $Y_{-L} = 1/S = 0.70$, contours $\Delta\Psi = 0.01$; d) $Y_{-L} = 1/S = 0.75$, contours $\Delta\Psi = 0.01$; e) $Y_{-L} = 1/S = 0.80$, contours $\Delta\Psi = 0.01$; f) $Y_{-L} = 1/S = 0.85$, contours $\Delta\Psi = 0.01$

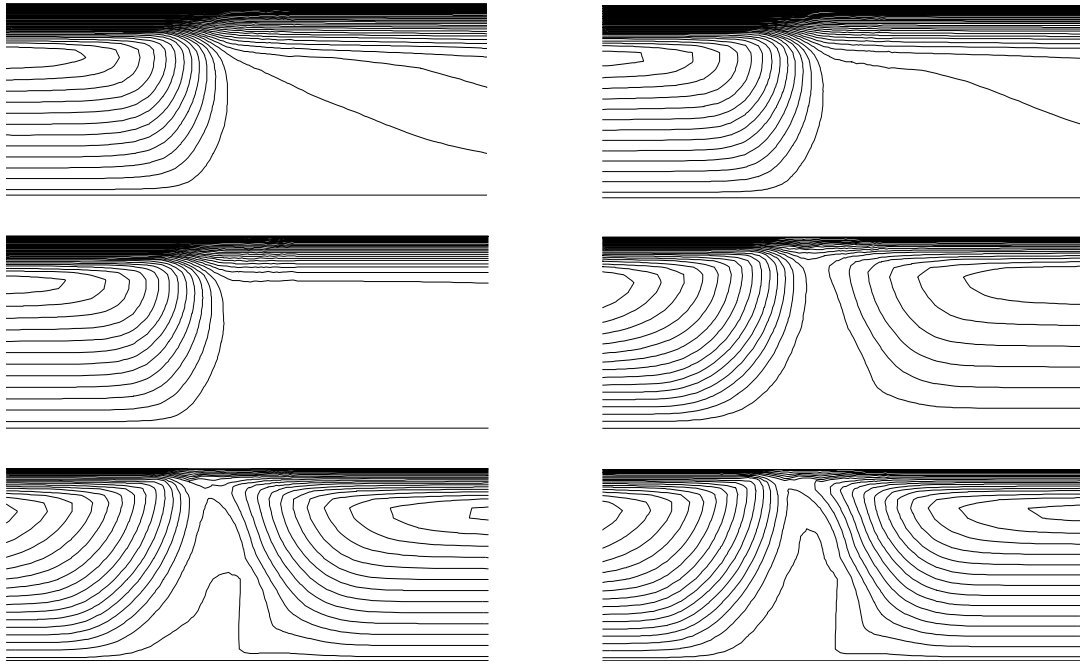


Fig. 5. Example computations for $(\tau_{c,Y}, \tau_{m,Y}, \mu_c, \mu_m) = (0.2, 0.5, 0.01, 0.05)$, showing the streamlines of the solution for different interface positions (left to right; top to bottom): a) $Y_{-L} = 1/S = 0.87$, contours $\Delta\Psi = 0.005$; b) $Y_{-L} = 1/S = 0.88$, contours $\Delta\Psi = 0.005$; c) $Y_{-L} = 1/S = 0.90$, contours $\Delta\Psi = 0.005$; d) $Y_{-L} = 1/S = 0.95$, contours $\Delta\Psi = 0.005$; e) $Y_{-L} = 1/S = 0.97$, contours $\Delta\Psi = 0.005$; f) $Y_{-L} = 1/S = 0.98$, contours $\Delta\Psi = 0.005$

fact a weak recirculation downstream of the region shown in fluid m . This feature is more evident in Figs. 5c and d. When the recirculation zone exists in Ω_m , a second streamline $\Psi = 0$ enters Ω_m at the downstream boundary $x_1 = L$. It appears that both this streamline and the upstream $\Psi = 0$ (i.e. the interface), intersect the x -axis. The significance of the emerging recirculation zone is that when $h_{\text{circ}} < h_{\text{max}}$, the static layer thickness that is observed to result from fully transient two-dimensional displacement computations is found to be given approximately by $h = h_{\text{circ}}$. For example, $h \approx 0.145 \approx h_{\text{circ}}$ for the computation shown in Fig. 1a. This approximate prediction of h has been observed for a great many computational results and the prediction also follows parametric variations remarkably well, see in [3].

In Figs. 5d–5f, we straddle the limit $h = h_{\text{min}} \approx 0.0323$. For progressively thin static layers below $h = h_{\text{circ}}$, we appear to attain a critical thickness at which the streamline $\Psi = 0$ entering at $x_1 = -L$ exits at $x_1 = L$, without intercepting the x_1 -axis, see Figs. 5e and 5f. At the same time, a second $\Psi = 0$ is observed in Figs. 5e–5f to bifurcate from the x_1 -axis and then rejoin it. It would appear that in this range of layer thicknesses, although the solutions converge numerically, the streamlines $\Psi = 0$ that are computed do not represent a physically plausible fluid-fluid interface. It is also worth noting that we are unable using the numerical code, to check how well the condition $\mathbf{u} \cdot \mathbf{n} = 0$ is satisfied on the interface.

Although not predicted particularly well by the numerical results, we believe that a second *critical* layer thickness is defined by h_{min} , i.e., that we cannot typically find a physically sensible steady solution with a static wall layer for $h < h_{\text{min}}$. The direct physical interpretation of (79) is that the unyielded region of the far-field displacing fluid flow is moving faster than the unyielded region of the displaced fluid, far downstream. In the case when (79) is satisfied, fluid m is being *pushed* by fluid c . In contrast, when (79) is not met (i.e. $h < h_{\text{min}}$), the unyielded region of fluid m far downstream is *pulling* that of fluid c , which makes it less likely that a steadily propagating interface can exist, separating the two fluids. In the case presented it appears this *critical* layer thickness has been attained for h slightly larger than h_{min} . We believe it is quite hard to resolve this limit with the numerical methods that we have used. Our choice of numerical methods has been intended mainly to provide example computations fairly simply and there is much room for improvement. The main numerical difficulty here seems to be that the layers are becoming thin relative to the mesh size and that h_{min} is also typically quite small. To get larger h_{min} we would need to consider small ratios of φ_μ , but from our existence results, these limits are also likely to give the most problems in terms of computing the solution. Our tentative conclusion is that physically sensible velocity solutions with a static wall layer should be computable for $h \in (h_{\text{min}}, h_{\text{max}})$, but not outside this interval.

6. Concluding remarks

We have considered the steady propagation of a finger of one Bingham fluid through another *thicker* Bingham fluid, filling the space between two parallel plates. It has been shown that fully two-dimensional steady solutions to this

problem exist, in cases where a uniform static residual layer of the displaced fluid is left on the walls of the slot. The type of interface for which such solutions have been shown to exist are those which are parallel to the slot axis at the inflow, are sufficiently smooth, and are those which, if they approach the slot axis perpendicularly, become perpendicular to the slot axis only sufficiently close to the slot axis. For each such suitable interface, subject to certain conditions on the ellipticity of the problem, the solution will be unique. However, the interface position is not unique. First of all, considerable variation in the shape of the interface close to $x_1 = 0$. Secondly, the far-field static layer thickness h can be selected arbitrarily in (h_{\min}, h_{\max}) . Numerical results have been presented that indicate the variation of h_{\min} and h_{\max} with the rheological parameters and we have shown a series of steady state solutions that have been computed for $h \in (h_{\min}, h_{\max})$.

These results, of uniqueness of the steady solution for specified interface, but non-uniqueness of the interface specification, are quite commonplace for multi-fluid flows. A number of examples of nonuniqueness of steady solutions to two-fluid flows are given in [9]. Here we have the additional complications of the Bingham rheologies, but the problem remains essentially the same. One conclusion is that the steady problem alone, does not determine the static layer thickness that is selected by a transient displacement. However, much insight has been gained by studying the steady problem, in particular the identification and interpretation of the limit h_{\min} .

In [3] it has been shown that the limiting layer thickness at which fluid m begins to recirculate, h_{circ} , gives a good approximation to the static layer thickness selected by fully transient displacements that have a static wall layer. This is a largely empirical observation in [3]. By way of explanation in [3], it is argued that static layer thicknesses close to h_{circ} are likely to approximately minimise the visco-plastic dissipation, close to $x_1 = 0$, over the set of all feasible interfaces. Arguments such as this in fact only make sense when we are able to prove the existence of solutions to the steady propagation problem for a range of interface configurations, as done here.

There are a number of interesting extensions of this work. Firstly, it would be possible to compute the steady solution over a range of admissible interface shapes and attempt to minimise a suitable viscous dissipation functional. This could be compared with the results of transient computations. Secondly, it would be interesting to use this steady problem as the basic solution in investigating instability of the displacement front. For both these applications, it would be advisable to modify the numerical method used, for both greater flexibility and accuracy.

In proving the results of this paper, we have not attempted to derive functional analytic bounds that are sharp, nor do we always consider the *best* function spaces. This is certainly possible, but we feel also that it would be a slightly fruitless exercise. Firstly, by analogy with Newtonian fluid flows it is usually found that the bounds derived for existence and uniqueness results are quite conservative. Secondly, in deriving bounds such as those in lemmas 1 and 4, quantities such as $\min\{\mu_k\}$, $\max\{\mu_k\}$, and $\max\{\tau_{k,Y}\}$ appear. Thus, regardless of the sharpness of the functional bounds that we use, we must expect our results to be weaker when the fluid rheologies are distinctly different. Whether or not this represents an underlying problem with these flows is not clear, but we believe that this is so. Finally, we note that the bounds we derive for the ellipticity constant α will depend upon the function \mathbf{u}^* that we have constructed, and thus on the interface shape and far-field boundary conditions (parametrically, on h , B_c , and B_m). Although we have found one particular $\mathbf{u}^* \in \bar{\mathcal{V}}$, with which to homogenise the variational problem (41), we have no insight into whether or not other $\mathbf{v}^* \in \bar{\mathcal{V}}$ might be *better* with respect to our bounds.

A final comment here concerns the assumption of symmetry of the interface. Non-symmetric interfaces will be the norm in channels that are inclined and for which the fluid densities are different, e.g. in most situations that approximate the primary cementing of a casing into an oil well. The same problem can be straightforwardly formulated for these situations. For a steadily propagating interface we will now have a lower and an upper static wall layer thickness, say h_l and h_u . We can impose an upstream boundary conditions with two static wall layers, provided only that $\max\{h_l, h_u\} < h_{\max}$, where in an inclined slot h_{\max} depends parametrically on $\varphi_B \cos \beta$ in place of φ ; β denotes the deviation from vertical. We are also able to use essentially the same construction of $\mathbf{u}^* \in \bar{\mathcal{V}}$, and expect therefore to be able to prove existence and uniqueness of solutions. The physical meaning of (79) is the same for a non-symmetric steady displacement and this will lead to the condition $h_l + h_u > 2h_{\min}$. Further quick insight is not forthcoming and this is an area for ongoing research.

Acknowledgement

We are grateful to the management of Schlumberger for their permission to publish this paper. The work of Giuliano Sona was completed during an internship at Schlumberger. This internship was partly funded by the European Union through the Leonardo da Vinci Community Programme. The work of Ian Frigaard was carried out whilst employed by Schlumberger and the collaboration with Otmar Scherzer was initiated during a study visit funded by Schlumberger.

References

- 1 ADAMS, R. A.: Sobolev spaces. Academic, New York 1975.
- 2 ALEXANDROU, A. N.; ENTOV, V.: On the steady-state advancement of fingers and bubbles in a Hele-Shaw cell filled by a non-Newtonian fluid. *Europ. J. Appl. Math.* **8** (1997), 73–87.

- 3 ALLOUCHE, M.; FRIGAARD, I. A.; SONA, G.: Static wall layers in the displacement of two visco-plastic fluids in a plane channel. *J. Fluid Mech.* **424** (2000), 243–277.
- 4 CHEN, C.-Y.; MEIBURG, E.: Miscible displacements in capillary tubes. Part 2: Numerical simulations. *J. Fluid Mech.* **326** (1996), 57–90.
- 5 DUVAUT, G.; LIONS, J.-L.: *Inequalities in mechanics and physics*. Springer 1976.
- 6 FIDAP 1998, Chapters 3–7 and 13. In: *FIDAP 8 Theory Manual*. Fluent Inc.
- 7 GLOWINSKI, R.: *Numerical methods for nonlinear variational problems*. Springer-Verlag 1983.
- 8 GUILLOT, D.; HENDRIKS, H.; CALLET, F.; VIDICK, B.: Mud removal. In: NELSON, E. B. (ed.): *Well Cementing*. Ch. 5. Schlumberger Educational Services 1990.
- 9 JOSEPH, D. D.; RENARDY, Y. Y.: *Fundamentals of two-fluid dynamics. Part I: Mathematical theory and applications*. Springer 1993 (*Interdisciplinary Applied Mathematics* 3), pp. 27–43.
- 10 MINEEV-WEINSTEIN, M.: Selection of the Saffman-Taylor finger width in the absence of surface tension: an exact result. *Phys. Rev. Lett.* **80** (1998) 10, 2113–2116.
- 11 SAFFMAN, P. G.: Viscous fingering in Hele-Shaw cells. *J. Fluid Mech.* **173** (1986), 73.
- 12 SAFFMAN, P. G.; TAYLOR, G. I.: The penetration of a finger into a porous medium in a Hele-Shaw cell containing a more viscous liquid. *Proc. Roy. Soc. London* **A245** (1958), 312.
- 13 SMITH, D. K.: *Cementing*. SPE monograph series (Society of Petroleum Engineers 1987), chapter 6, pp. 82–106.
- 14 WILSON, S. D. R.: The Saffman-Taylor problem for a non-Newtonian liquid. *J. Fluid Mech.* **220** (1990), 413–425.
- 15 YANG, Z.; YORTSOS, Y. C.: Asymptotic solutions of miscible displacements in geometries of large aspect ratio. *Phys. Fluids* **9** (1997) 2, 286–298.

Received October 28, 1999, accepted February 8, 2000

Addresses: Dr. IAN FRIGAARD, Department of Mathematics and Department of Mechanical Engineering, University of British Columbia, 1984 Mathematics Road, Vancouver BC, Canada V6T 1Z2, e-mail: frigaard@interchange.ubc.ca; Prof. OTMAR SCHERZER, Angewandte Mathematik, Universität Bayreuth, D-95440 Bayreuth, Germany, e-mail: otmar.scherzer@uni-bayreuth.de; GIULIANO SONA, Dipartimento di Matematica, Università degli Studi, Viale Morgagni 67a, I-50134 Firenze, Italy